
LAGRANGE OSCILLATORY NEURAL NETWORKS FOR CONSTRAINT SATISFACTION AND OPTIMIZATION

Corentin Delacour¹ Bram Haverkort² Filip Sabo² Nadine Azemard¹ Aida Todri-Sanial^{1,2}

¹ Microelectronics Dept., LIRMM, University of Montpellier, CNRS, France

² Electrical Engineering Dept., Eindhoven Technical University, The Netherlands

ABSTRACT

Physics-inspired computing paradigms are receiving renewed attention to enhance efficiency in compute-intensive tasks such as artificial intelligence and optimization. Similar to Hopfield neural networks, oscillatory neural networks (ONNs) minimize an Ising energy function that embeds the solutions of hard combinatorial optimization problems. Despite their success in solving unconstrained optimization problems, Ising machines still face challenges with *constrained* problems as they can get stuck at infeasible local minima. In this paper, we introduce a Lagrange ONN (LagONN) designed to escape infeasible states based on the theory of Lagrange multipliers. Unlike existing oscillatory Ising machines, LagONN employs additional Lagrange oscillators to guide the system towards feasible states in an augmented energy landscape and settles only when constraints are met. Taking the maximum satisfiability problem with three literals as a use case (Max-3-SAT), we harness LagONN's constraint satisfaction mechanism to find optimal solutions for random SATlib instances with up to 200 variables and 860 clauses, which provides a deterministic alternative to simulated annealing for coupled oscillators. We further discuss the potential of Lagrange oscillators to address other constraints, such as phase copying, which is useful in oscillatory Ising machines with limited connectivity.

1 Introduction

Physics-inspired approaches to computing such as Ising machines are actively explored as potential efficient hardware solutions for data-centric applications like artificial intelligence or optimization [2]. Ising machines are closely related to the seminal works from Hopfield [3] and Tank [4] from the 1980s who introduced analog neural networks to *naturally* solve NP-hard problems in combinatorial optimization such as the traveling salesman problem (TSP). Given a list of cities and their coordinates, TSP consists of finding a minimum-distance tour that visits every city and returns to the initial city. Hopfield and Tank's original idea is to map cities and their position in the tour to analog neurons, and intercity distances to synaptic connections, such that the problem instance is "physically wired". Then, the neurons evolve in parallel to minimize an Ising-like energy that embeds the TSP tour distance. Despite the elegance of the approach, it is well known that the system state can get stuck at local energy minima corresponding to infeasible tours, e.g., two cities are visited simultaneously [5]. Enforcing such constraints is theoretically possible with sufficiently large penalty coefficients [6], at the expense of runtime to find optimal solutions due to the dominance of constraints in the energy function, which causes important slowdowns. Although in software it is possible to implement hard constraints by only producing feasible samples, Ising machines rather implement *soft* constraints embedded in the energy function. Hence, the current approach for solving constrained optimization problems with Ising machines is to optimize the penalty strength as a trade-off between satisfiability and accuracy [7–9].

Given this energy function, what other tricks can we use to ensure constraint satisfaction, apart from setting impractical large penalty parameters? Owing to their continuous energy landscape, analog systems seem to offer additional techniques compared to their digital counterparts. In particular, they fit well with the formalism from Lagrange for constrained optimization on continuous functions [10, 11], which is a common principle to various physics-based solvers [12]. By relaxing the Ising energy to a continuous energy landscape, it is possible to apply Lagrange's theory

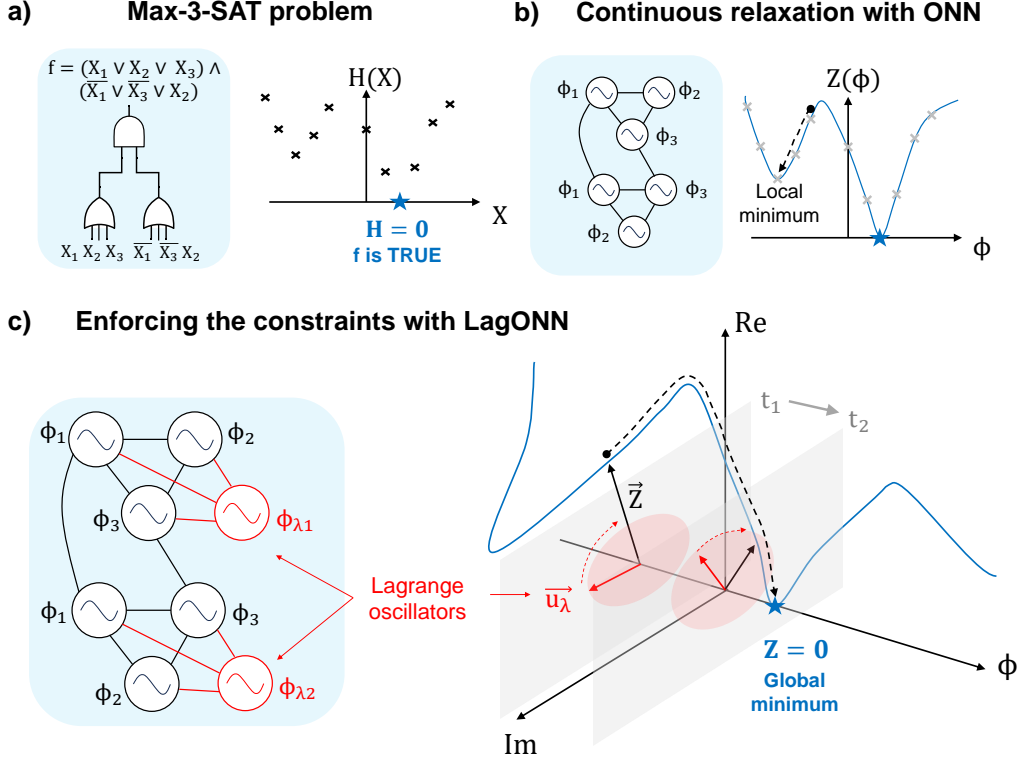


Figure 1: a) Any combinatorial optimization problem can be mapped to the 3-SAT problem [1]. Its optimization version Max-3-SAT seeks an assignment X satisfying most clauses and can be described as the minimization of an Ising energy function $H(X)$. b) Phase-based oscillatory neural networks (ONN) are analog solvers for combinatorial optimization. Their energy function $E(\phi)$ corresponds to a continuous relaxation of $H(X)$. ONNs can get stuck at local energy minima. c) The proposed Lagrange ONN employs additional oscillators to enforce constraint satisfaction corresponding to 3-SAT clauses. Conceptually, these forces correspond to vectors \vec{u}_λ that "push" an energy vector \vec{Z} along new directions to escape local minima and reach an optimal solution.

and prevent the system state from relaxing to infeasible solutions, and rather force it to escape infeasible energy minima using additional variables — Lagrange multipliers λ [13]. Conceptually, the dynamics consist of a competition between a gradient descent along the original variable direction (to minimize a cost function) and an ascent along the λ direction (to enforce the constraints). Another interesting property of continuous variables is the parallel system evolution, contrasting with the typical sequential nature of simulated annealing [14], based on Gibbs sampling and only allowing sequential moves between connected spins.

In this paper, we revisit the concept of Lagrange multipliers applied to coupled phase oscillators labeled *Lagrange oscillatory neural network* (LagONN), and illustrated in Fig.1. This platform choice is motivated by the recent coupled oscillators developments [15] that have shown promising results in solving hard combinatorial optimization problems in the analog domain, such as the Maximum cut problem [16–20], Satisfiability (SAT) [21], and the Maximum independent set problem [22]. Moreover, dense implementations of coupled oscillators using CMOS technology are already available [19, 23–25], and emerging technologies like spintronic devices [26, 27] or transition-based and bistable devices [28–31] promise further scaling. Our primary objective in this work is to showcase constraint satisfaction with coupled phase oscillators without using quadratic energy penalties [6], thus avoiding the trade-off between feasibility and accuracy in constrained optimization problems.

As a first step, we choose a pure satisfaction problem as a use case, the Max-3-SAT problem, whose hardware acceleration has been extensively explored in literature due to the problem's versatility [32–37]. The objective is to find a Boolean assignment of variable x that maximizes the number of TRUE clauses composed of three literals $C_m = l_1^m \vee l_2^m \vee l_3^m$ in the formula:

$$f_B = C_1 \wedge C_2 \wedge \dots \wedge C_{M-1} \wedge C_M \quad (1)$$

With $l_j^m \in \{x_1, \dots, x_N, \overline{x_1}, \dots, \overline{x_N}\}$. The problem of assessing whether or not f_B is satisfiable is NP-complete [1], thus any problem in NP can be reduced to 3-SAT in theory. From the Ising machine point of view, we may want to define an Ising energy combining terms from all clauses, and the objective would be to find its ground state (Fig.1b). Another view that we explore in this work and closer to the original Max-3-SAT formulation is to interpret the problem as maximizing the number of satisfied constraints, which naturally leads to a Lagrange formulation [13].

Interestingly, since the Lagrange formalism provides a deterministic mechanism to escape *infeasible* states based on constraint satisfaction, this translates into a ground state search for pure satisfaction problems like Max-3-SAT for which other classical solvers can get stuck at local minima (Fig.1c). Hence, in this case, LagONN constitutes a deterministic alternative to stochastic algorithms for ground state search such as simulated annealing [14]. This is an interesting feature for oscillatory-based Ising machines as harnessing noise and annealing can be challenging in practice.

The paper is organized as follows. After discussing prior work on physics-inspired solvers, we introduce a Lagrange oscillatory neural network (LagONN) that maps a 3-SAT formula to interconnected oscillatory subcircuits whose dynamics seek an optimal saddle point in the energy landscape satisfying all constraints. Next, we benchmark LagONN against simulated annealing on Max-3-SAT instances from the SATlib library up to 200 variables and 860 clauses [38]. Finally, we discuss how Lagrange oscillators could be used for other constrained optimization problems, such as copying phases in hardware with limited connectivity.

2 Background

2.1 Physics-inspired solvers for combinatorial optimization

At the heart of many physics-inspired solvers for combinatorial optimization, a common idea is to map the problem cost function to an energy, often set as the Ising Hamiltonian and expressed as:

$$H = - \sum_{i < j} J_{ij} S_i S_j - \sum_i h_i S_i \quad (2)$$

where $S_i = \pm 1$ are the spins, J_{ij} the interaction coefficients between spins, and h_i is the external field applied to spin S_i . Finding the ground states of H is in general NP-hard [6]. Updating a spin value S_i causes an energy change ΔH_i that can drive the search in the energy landscape. While a deterministic search based only on energy minimization will likely get stuck at local minima, most state-of-the-art approaches allow some energy increase with nonzero probability to escape local minima. The common choice for the system probability distribution is the Boltzmann law $\pi = \exp(-H/T)/Z$ that assigns high probabilities to low-energy states where T is a temperature parameter and Z is the partition function. Using Markov chain Monte Carlo algorithms such as Gibbs sampling, one can then sample from the Boltzmann distribution by updating each spin sequentially, based on its local information $I_i = \sum_j J_{ij} S_j + h_i$ [39]. Since for combinatorial optimization the goal is to find low-energy states, the simulated annealing algorithm [14] is a great choice for hardware implementation with noisy devices such as memristor arrays [40] or coupled probabilistic bits (p-bits) that naturally produce probabilistic spin updates [41]. Implementing Gibbs sampling with synchronous systems typically imposes a sequential spin update, although this is not a limitation for asynchronous systems [42] or sparse hardware with high parallelism [43]. In this paper, the system state components evolve in parallel owing to dynamics determined by differential equations. Our model is deterministic, although our numerical integration scheme introduces some errors, as discussed in the Appendix B.

At first sight, a deterministic search may seem unsuitable for exponentially large spaces since the system state follows a determined trajectory and cannot "jump" in the state space to speed up the search like simulated annealing. A deterministic algorithm thus greatly depends on initialization and the system may take exponential time before reaching an optimal point. However, this feature is also common to simulated annealing since cooling during a *finite* duration can freeze the variables to sub-optimal solutions [44]. Other adiabatic approaches consisting of slowly annealing the energy landscape are not exempt from this issue [45, 46]. These techniques can be thought of as "shaping" the energy landscape during annealing, which in practice means adapting the coupling amplitudes $|J_{ij}|$ in real-time. In our approach, the weight amplitude $|J_{ij}|$ is rather fixed but its *phase* θ_{ij} varies in real-time, which can also be seen as an adaptive energy landscape.

Finally, many deterministic solvers are based on custom differential equations [47–50] where the system phase space contains attractors corresponding to solutions, or purposely introduces chaos to mimic Boltzmann sampling [51, 52]. To build a corresponding physical machine, a crucial feature of these models is whether the system has bounded variables or not. In [47] and [53], the authors propose an analog model that provides an exponential speed-up at the expense of unbounded variables and hence a potential exponential power. In contrast, limiting the growth of variable values generally induces an exponential computation time for hard instances [48]. In this work, we restrict ourselves

to dynamics that are implementable by coupled phase oscillators, which guarantees a bounded circuit power since variables are phases and the synaptic amplitudes $|J_{ij}|$ are fixed.

2.2 Computing with analog oscillatory neural networks

This work focuses on oscillatory neural networks that compute in the phase domain, i.e. we assume that all oscillators have the same frequency, so information can be encoded in oscillator phases ϕ_i measured against a reference oscillator. Under this assumption and when synaptic weights are symmetric $J_{ij} = J_{ji}$, coupled oscillators are known to minimize an Ising-like energy and thus are very similar to analog Hopfield neural networks [54–56]. Harnessing phase dynamics for combinatorial optimization was brought up to date thanks to the seminal work from Wang et al. [57] who formally linked phase dynamics to the Ising model (Eq. 2). With sinusoidal interactions, the oscillatory neural network energy can be thought of as a two-dimensional XY Ising Hamiltonian expressed as:

$$E = - \sum_{i < j} J_{ij} \cos(\phi_i - \phi_j) - \sum_i h_i \cos(\phi_i) \quad (3)$$

which is a relaxation of the one-dimensional Ising model since $E = H$ for binary phases (multiple of π). While the continuous nature of phases in E is harnessed in efficient Max-Cut solvers [58, 59], most coupled-oscillator studies focus on the binary Ising model and inject harmonic signals to binarize phases as proposed in [17]. In this paper, we do not use an additional binarization mechanism as we will see that the fixed points tend to have binary phases.

In [21], the authors further extended the energy E to hypergraphs involving high-order interactions between the variables, whereas the classical Ising model (Eq. 2) has only spin-to-spin quadratic interactions. With this extension, one can map some NP-hard problems such as Satisfiability directly to the hardware without *quadrization* that adds auxiliary oscillators [60]. This article focuses on this approach and in particular, we are interested in a simultaneous interaction between four oscillators k, l, m, n whose energy can be expressed as:

$$E_{klmn} = J_{kl} \cos(\phi_k - \phi_l + \phi_m - \phi_n) = \text{Re} \left(J_{kl} \exp [i(\phi_m - \phi_n)] \exp [i(\phi_k - \phi_l)] \right) \quad (4)$$

Looking at Eq. 4, the additional 3rd and 4th order interactions m and n can be interpreted as a complex synapse connecting k and l with amplitude J_{kl} and synaptic phase $\theta_{kl} = \phi_m - \phi_n$ carrying the high order information from m, n , that can also be interpreted as delay $\tau_{kl} = (\phi_m - \phi_n)/\omega_0$ where ω_0 is the oscillating frequency. Having 4th-order interactions, the three variables of a 3-SAT clause plus an additional Lagrange variable could interact simultaneously. We are aware that implementing such high-order interaction is not straightforward and we leave it as future work, although some ideas are discussed in Section 3.2.

2.3 Constrained optimization with Lagrange multipliers

This paper harnesses the concept of Lagrange multipliers that are at the heart of various techniques for constrained optimization problems [10, 11, 61, 62]. Given a cost function $f(x)$ and constraints $g(x)$, most of these methods are based on a Lagrange function defined as:

$$L(x, \lambda) = f(x) + \lambda^T g(x) \quad (5)$$

where the constraints are satisfied when $g(x) = 0$, and λ is a new variable called *Lagrange multiplier*. Similar to the penalty method [10], the Lagrange method weights the constraints and adds them to the cost function. The minimum of L with respect to x is then a lower bound for the optimal constrained solution $f(x^*)$ as $\min_x L \leq L(x^*, \lambda) = f(x^*)$. The purpose of the Lagrange multiplier λ is to close the gap, i.e. to find an optimal λ^* satisfying $\min_x L(x, \lambda^*) = f(x^*)$, or to reduce the gap as maximum to have the tightest lower bound on the optimal value [61]. Since L is a concave function of λ [63], the optimal λ^* can be found by maximizing $\min_x L$ as:

$$L^* = \max_{\lambda} \min_x L(x, \lambda) \quad (6)$$

For continuous functions f and g , it is possible to interpret this optimization problem as a Lagrange neural network as defined in [64] where neurons perform gradient descent along x to minimize L , while Lagrange neurons perform gradient ascent in the λ -direction to reduce the gap (Eq. 6) and reach an optimal solution $f(x^*)$ that satisfies the constraints. The corresponding dynamics could be:

$$\begin{cases} \tau \dot{x} = -\nabla_x L \\ \tau_{\lambda} \dot{\lambda} = +\nabla_{\lambda} L = g(x) \end{cases} \quad (7)$$

where τ and τ_{λ} set the minimization and maximization speed, respectively. Reaching the global optimum $f(x^*)$ requires an ideal minimizer, and in non-convex settings gradient descent can get stuck in local minima and lead to suboptimal

solutions. However, it is interesting to note that the search for a constrained solution *cannot* stop until the constraints are met as $g(x) = 0$. Hence, for satisfaction problems such as Max-3-SAT that we explore in this paper, the search does not stop until all clauses are TRUE. Another geometric interpretation of the dynamics defined as Eq. 7 is the search for a saddle point of L , that is a minimum and maximum of L in the x and λ -directions, respectively. Generally, the energy landscape is non-convex and L^* is not necessarily a saddle point [63]. For LagONN, we show next that for satisfiable instances, L^* is a saddle point meeting the constraints and can be found with competitive dynamics as defined in Eq. 7.

3 Results

3.1 An oscillatory-based Lagrange multiplier for 3-SAT

We propose a similar idea to Nagamatsu et al. [13] for solving the Max-3-SAT problem (Eq. 1) using a Lagrange neural network with phase-based oscillatory neurons. We first express a clause C_i as an Ising energy H_i that is 0 if and only if C_i is true. For 3-SAT, there are four possible clauses that we map to an Ising energy as follows:

$$\begin{aligned} C_1 = X \vee Y \vee Z &\longrightarrow H_1 = 1 + S_X S_Y + S_X S_Z + S_Y S_Z - (S_X + S_Y + S_Z) - S_X S_Y S_Z \\ C_2 = \bar{X} \vee Y \vee Z &\longrightarrow H_2 = 1 - S_X S_Y - S_X S_Z + S_Y S_Z - (-S_X + S_Y + S_Z) + S_X S_Y S_Z \\ C_3 = \bar{X} \vee \bar{Y} \vee Z &\longrightarrow H_3 = 1 + S_X S_Y - S_X S_Z - S_Y S_Z - (-S_X - S_Y + S_Z) - S_X S_Y S_Z \\ C_4 = \bar{X} \vee \bar{Y} \vee \bar{Z} &\longrightarrow H_4 = 1 + S_X S_Y + S_X S_Z + S_Y S_Z + (S_X + S_Y + S_Z) + S_X S_Y S_Z \end{aligned} \quad (8)$$

where spins $S_j = \pm 1$ are the binary Ising variables with $S_j = +1$ corresponding to TRUE. Writing the truth table for each clause, we find that C_i is TRUE when $H_i = 0$ and C_i is FALSE when $H_i = 8$. The next step is to map the Ising energies to phase-based oscillatory neural networks. We propose to relax the binary Ising Hamiltonians to complex variables defined as:

$$\begin{aligned} H_1 &\longrightarrow Z_1 = 1 + e^{i(\phi_X - \phi_Y)} + e^{i(\phi_X - \phi_Z)} + e^{i(\phi_Z - \phi_Y)} - (e^{i\phi_X} + e^{i\phi_Y} + e^{i\phi_Z}) - e^{i(\phi_X - \phi_Y + \phi_Z)} \\ H_2 &\longrightarrow Z_2 = 1 - e^{i(\phi_X - \phi_Y)} - e^{i(\phi_X - \phi_Z)} + e^{i(\phi_Z - \phi_Y)} - (-e^{i\phi_X} + e^{i\phi_Y} + e^{i\phi_Z}) + e^{i(\phi_X - \phi_Y + \phi_Z)} \\ H_3 &\longrightarrow Z_3 = 1 + e^{i(\phi_X - \phi_Y)} - e^{i(\phi_X - \phi_Z)} - e^{i(\phi_Z - \phi_Y)} - (-e^{i\phi_X} - e^{i\phi_Y} + e^{i\phi_Z}) - e^{i(\phi_X - \phi_Y + \phi_Z)} \\ H_4 &\longrightarrow Z_4 = 1 + e^{i(\phi_X - \phi_Y)} + e^{i(\phi_X - \phi_Z)} + e^{i(\phi_Z - \phi_Y)} + (e^{i\phi_X} + e^{i\phi_Y} + e^{i\phi_Z}) + e^{i(\phi_X - \phi_Y + \phi_Z)} \end{aligned} \quad (9)$$

We purposely introduce phase differences, e.g. $\phi_X - \phi_Y$, to have a complex relaxation Z_i of the conventional coupled-oscillators energy function (Eq. 3). By construction, the complex relaxation Z_i equals the Hamiltonian H_i for binary phases $\phi_j = \pi(1 - S_j)/2$. Unfortunately, there could be non-binary phases such that $Z_i = 0$ where assigning phases to Ising spins is non-obvious. Note the high-order interaction terms do not cause this but is rather inherent from the two-dimensional nature of the XY Ising model. This situation is similar to solving the Max-cut problem with coupled oscillator systems without forcing binarization [17, 20]: it opens the question of how to round phases to spins. In this work, however, we will see that when there are more than a few clauses, the phase fixed points tend to be binary. Using this property, the idea is to have a coupled oscillator module that minimizes $|Z_i|$ so that when $Z_i = 0$, the phases ϕ_X , ϕ_Y , and ϕ_Z give the values for the Boolean variables S_X , S_Y , and S_Z that satisfy clause C_i .

Constraining the oscillators for reaching $Z_i = 0$ can be expressed using the Lagrange function $L_i(\phi, \lambda)$ as follows:

$$L_i(\phi, \lambda) = \lambda_R \text{Re}[Z_i] + \lambda_I \text{Im}[Z_i] \quad (10)$$

We indeed have $\nabla_\lambda L_i = (\text{Re}[Z_i], \text{Im}[Z_i]) = 0 \iff Z_i = 0$. Note that there are only two constraints and no cost function f compared to the general case of the Lagrange multiplier method (Eq. 5). It is then a pure constraint satisfaction problem with the constraint function $g = (\text{Re}[Z_i], \text{Im}[Z_i]) = 0$. There are two possible interpretations for the Lagrange multipliers, leading to two different types of Lagrange oscillatory neural networks:

1. λ_R and λ_I are *synaptic elements*. This possibility opens up the question of how to implement synapses λ_R and λ_I that need to evolve in real-time while having a limited range for a real implementation.
2. λ_R and λ_I are *oscillatory variables*, i.e. phase oscillators. This interpretation only involves oscillating neurons and synapses with fixed amplitude, potentially facilitating the hardware implementation.

Focusing on the second interpretation, a particular choice for λ simplifies the Lagrange function L_i (Eq.10). We consider a Lagrange *oscillator* with the same frequency as the other neurons, phase ϕ_λ , and unit amplitude (Fig. 2b). While moving in the 2D plan, the corresponding unit vector \vec{u}_λ has coordinates $(\cos \phi_\lambda, \sin \phi_\lambda)$ that we assign to

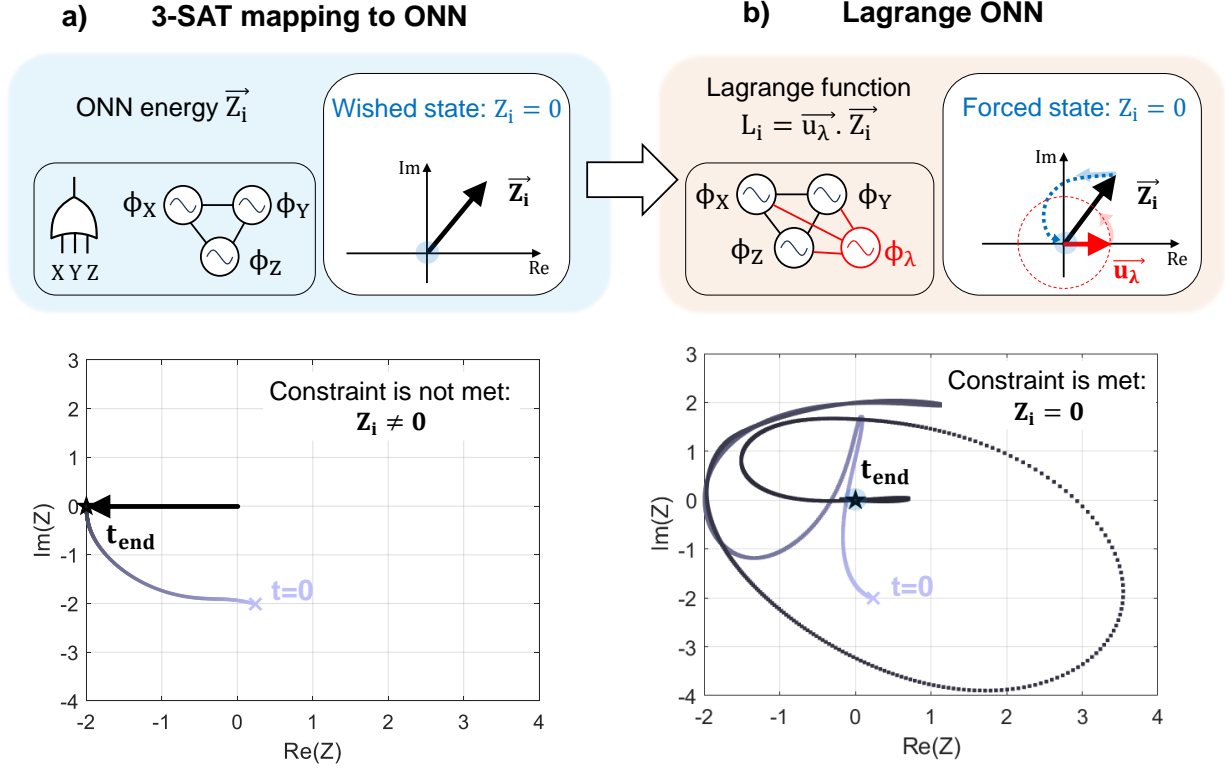


Figure 2: a) 3-SAT clause mapping to ONN. The Ising energy is relaxed to a complex quantity Z_i , a function of ONN phases ϕ_X, ϕ_Y, ϕ_Z . For binary phases, $Z_i = 0$ reduces the optimal Ising state and induces $C_i = \text{TRUE}$. However, the standard ONN trajectory settles to an undesired fixed point where $Z_i \neq 0$ (bottom). b) Adding a Lagrange oscillator with phase ϕ_λ can force the constraint $Z_i = 0$. This is achieved by defining the Lagrange function L_i and setting competitive dynamics (gradient descent and ascent) seeking a saddle point of L_i where $Z_i = 0$. Bottom: resulting Lagrange ONN trajectory for the same phase initialization.

multipliers (λ_R, λ_I) . Hence, the resulting Lagrange function becomes the dot product between \vec{u}_λ and the vector $\vec{Z}_i = (\text{Re}[Z_i], \text{Im}[Z_i])$ as:

$$L_i(\phi, \phi_\lambda) = \vec{u}_\lambda \cdot \vec{Z}_i = \cos \phi_\lambda \text{Re}[Z_i] + \sin \phi_\lambda \text{Im}[Z_i] \quad (11)$$

This leads to a compact expression for L_i as shown here for the first type of clause $i = 1$:

$$\begin{aligned} L_1(\phi, \phi_\lambda) = & \cos \phi_\lambda \\ & - \cos(\phi_X - \phi_\lambda) - \cos(\phi_Y - \phi_\lambda) - \cos(\phi_Z - \phi_\lambda) \\ & + \cos(\phi_X - \phi_Y - \phi_\lambda) + \cos(\phi_X - \phi_Z - \phi_\lambda) + \cos(\phi_Z - \phi_Y - \phi_\lambda) \\ & - \cos(\phi_X - \phi_Y + \phi_Z - \phi_\lambda) \end{aligned} \quad (12)$$

We recognize the energy function of four sinusoidal coupled oscillators $\phi_X, \phi_Y, \phi_Z, \phi_\lambda$ with high-order interactions up to four as shown by the last term [21]. Interestingly, the synaptic amplitudes appear as fixed binary weights ± 1 for the cosine terms. Hence, this ensures having bounded LagONN variables since only phases vary and are bounded by definition. Introducing an oscillatory Lagrange multiplier creates a saddle point in the energy landscape where the constraint $Z_i = 0$ is met, as shown in the next theorem.

Theorem 1. Let $L_i(\phi, \phi_\lambda) = \vec{u}_\lambda \cdot \vec{Z}_i$ then:

1. L_i has at least one saddle point $L_i(\phi^*, \phi_\lambda^*) = 0$ such that $L_i(\phi^*, \phi_\lambda) \leq L_i(\phi^*, \phi_\lambda^*) \leq L_i(\phi, \phi_\lambda^*)$.
2. Such saddle point satisfies the constraint $Z_i(\phi^*) = 0$.

The theorem is proven in Appendix D. Since LagONN's energy landscape $L_i(\phi, \phi_\lambda)$ has at least one saddle point satisfying the constraint, we set the phase dynamics for ϕ such that it minimizes $L_i(\phi, \phi_\lambda)$ and simultaneously, the

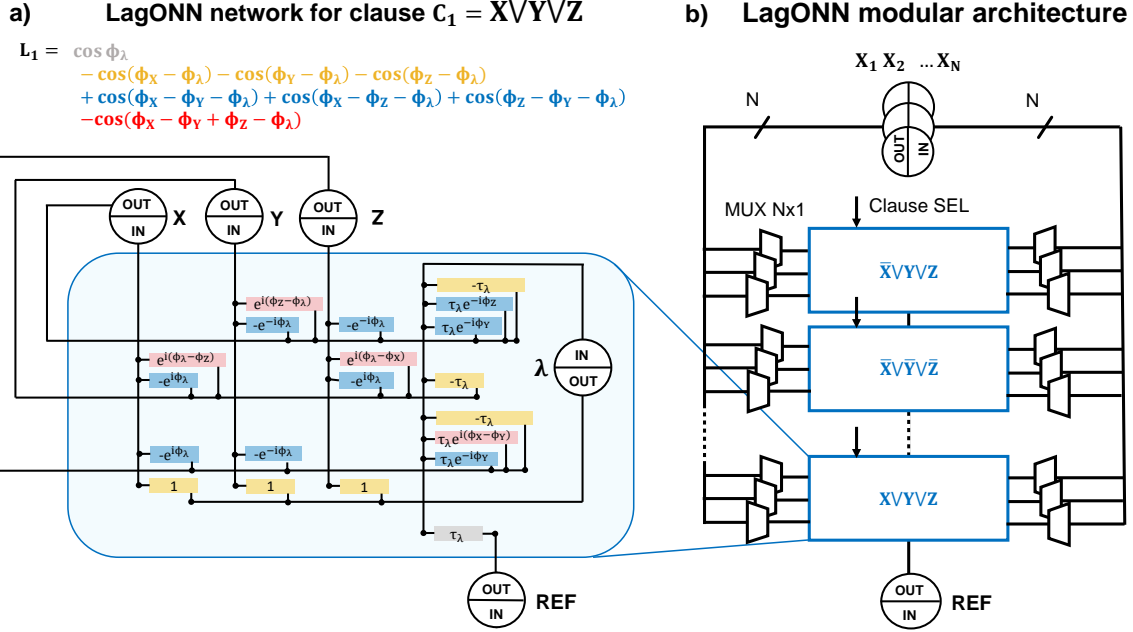


Figure 3: a) LagONN network for solving clause C_1 . Rectangles denote complex synapses in the form $J_{ij} \exp(i\theta_{ij})$ where θ_{ij} is implemented with a delay θ_{ij}/ω_0 in practice. The connections for θ_{ij} are not shown. b) Modular LagONN architecture to program any 3-SAT formula f_B with N variables and M clauses. Each rectangle corresponds to a clause subcircuit and contains a Lagrange oscillator. The clause selection signal programs the clause subcircuit to one of the four possible clauses. $N \times 1$ multiplexers route oscillator input and output signals to each clause according to the desired Boolean formula f_B .

Lagrange oscillator with phase ϕ_λ maximizes $L_i(\phi, \phi_\lambda)$, hoping to reach a saddle point where $Z_i(\phi^*) = 0$ as shown in Fig.2b. Overall, we propose the following phase dynamics for a clause C_i :

$$\begin{cases} \tau \dot{\phi}_j = -\nabla_{\phi_j} L_i(\phi, \phi_\lambda) = -\vec{u}_\lambda \cdot \partial \vec{Z}_i / \partial \phi_j \\ \tau_\lambda \dot{\phi}_\lambda = +\nabla_{\phi_\lambda} L_i(\phi, \phi_\lambda) = \vec{u}_\lambda \cdot \vec{Z}_i \end{cases} \quad (13)$$

where τ and τ_λ are the time constants for the standard and Lagrange oscillators, and $\vec{u}_\lambda = (-\sin \phi_\lambda, \cos \phi_\lambda)$. The time constants define the relative speed between gradient descent and ascent that we set to $\tau = \tau_\lambda$ as it provides faster convergence in simulations (see Appendix E). The dynamics can be thought of as a *competition* between \vec{Z}_i and \vec{u}_λ where the desired outcome is reaching $Z_i = 0$ as a compromise (L_i 's optimal saddle point) between the two competitive dynamics. Fig.2 shows examples of oscillatory neural network dynamics without and with a Lagrange oscillator. In the absence of Lagrange oscillator, the phases evolve to minimize $\text{Re}[Z_i]$ and settle to an undesired fixed point where $Z_i = -2$ (Fig.2a). However, the wished state is $Z_i = 0$ (Eq. 9) that would satisfy the clause C_i for binary phases. By introducing a Lagrange oscillator as defined in Eq. 12 with competitive dynamics, the phases are now constrained to reach a saddle point. An example of LagONN dynamics is shown in Fig.2b for the same initialization, highlighting the complex dynamics resulting from the competitive behavior. Eventually, the system settles to an optimal saddle point where $Z_i = 0$. Note that the Lagrange function (Eq. 11) is not a Lyapunov function for the system as it can increase with time (see Appendix D).

3.2 Modular architecture for 3-SAT formula

A LagONN network implementing the dynamics in Eq. 13 for $C_1 = X \vee Y \vee Z$ is shown in Fig.3a. There is a reference oscillator to measure the phases and apply an external field to the Lagrange oscillator. Thus, ϕ_j corresponds to $\phi_j - \phi_{REF}$ in practice. The LagONN network complexity mostly originates from the synaptic array that consists of delayed and weighted signals. In Fig.3a, we denote a synapse S_{ij} that connects oscillators i and j with weight W_{ij} and phase θ_{ij} as $S_{ij} = W_{ij} e^{i\theta_{ij}}$. This supposes having a mechanism to delay the synaptic input by θ_{ij}/ω_0 in real-time, which is the consequence of the fourth-order interaction terms in the LagONN function (Eq. 12). We believe

Table 1: Comparison between two possible LagONN architectures.

LagONN architecture	Fully-connected	Modular
Oscillators	$N + M$	$N + M$
Size of synaptic array	$(N + M)^2$	$4^2/\text{module (clause)}$
Distance of high-order interaction	$N + M$ (global)	4 (local)
$N \times 1$ multiplexers	0	$6M$

this scheme is compatible with mixed-signal ONNs [20, 24] that could use digital synchronization circuits such as latches or counters to propagate the phase information from the third and fourth oscillators. Another approach would be to modulate the synaptic current amplitude between two oscillators in real-time with phases from two others. Such circuitry would probably be composed of analog amplifiers that are compatible with all kinds of analog oscillators, such as spintronic-based [26] or relaxation oscillators [20, 28, 65].

We now consider a larger Boolean formula f_B with N Boolean variables and M clauses $C_m = l_1^m \vee l_2^m \vee l_3^m$ defined as:

$$f_B = C_1 \bigwedge C_2 \bigwedge \dots \bigwedge C_{M-1} \bigwedge C_M \quad (14)$$

with $l_j^m \in \{x_1, \dots, x_N, \overline{x_1}, \dots, \overline{x_N}\}$. The 3-SAT instance can be mapped to LagONN modules where a module m corresponds to a clause C_m , and each literal l_j^m corresponds to an input port of a module m (Fig.3b). A module corresponds to the network shown in Fig.3a and is highlighted by the blue box. Implementing the AND operation " \bigwedge " between two clauses is unnecessary as every Lagrange oscillator evolves to satisfy its corresponding clause. Thus, the whole network maximizes the number of TRUE clauses in f_B . We connect the LagONN modules as follows. If two clauses m and n have a literal in common at positions k and l : $l_k^m = l_l^n$ or $l_k^m = \overline{l_l^n}$ corresponding to variable ϕ_{x_j} , $j \in \{1, \dots, N\}$, then we connect input ports k and l to connect each set of synapses from clauses m and n to ϕ_{x_j} . Repeating this procedure for every pair of clauses, every variable ϕ_{x_j} sees the influence from all its corresponding clauses, and the total LagONN function becomes:

$$L_T(\phi_x, \phi_\lambda) = \sum_{m=1}^M u_\lambda^m \cdot \vec{Z}_m(\phi_x) \quad (15)$$

where ϕ_x is the vector of phases corresponding to the Boolean variables $\phi_x = (\phi_{x_1}, \phi_{x_2}, \dots, \phi_{x_{N-1}}, \phi_{x_N})^T$ and ϕ_λ contains all the Lagrange variables as $\phi_\lambda = (\phi_{\lambda_1}, \phi_{\lambda_2}, \dots, \phi_{\lambda_{M-1}}, \phi_{\lambda_M})^T$. The proposed modular architecture has two main advantages. First, it avoids implementing large synaptic arrays as synapses are contained in modules. Second, it maintains the synaptic high-order interactions locally inside the modules. In contrast, a programmable fully-connected design with $N + M$ oscillators would require a $(N + M)^2$ synaptic array to support any f_B instance. Moreover, it seems very challenging to propagate the high-order interaction throughout the whole synaptic array as not directly possible with a standard array laid out as a two-dimensional grid. However, we note that another kind of two-dimensional array appears with the programmable modular approach. Since each module input/output can be connected to N different input/output lines, a programmable architecture would require $6M N \times 1$ multiplexers. Compared to a fully connected design, there is a trade-off between the overhead from multiplexers vs. the complexity of propagating high-order interactions. The comparison between the modular and fully connected LagONN architectures scaling is summarized in Table 1.

3.3 LagONN dynamics

Assuming that the formula f_B is satisfiable, we extend Theorem 1 to the total Lagrange function L_T with M clauses.

Theorem 2. Let $L_T(\phi, \phi_\lambda) = \sum_m^M u_\lambda^m \cdot \vec{Z}_m$ and the formula $f_B = C_1 \bigwedge C_2 \bigwedge \dots \bigwedge C_{M-1} \bigwedge C_M$ is satisfiable, then:

1. L_T has at least one saddle point $L_T(\phi^*, \phi_\lambda^*) = 0$ such that $L_T(\phi^*, \phi_\lambda) \leq L_T(\phi^*, \phi_\lambda^*) \leq L_T(\phi, \phi_\lambda^*)$.
2. Such saddle point satisfies the constraints $Z_m(\phi^*) = 0$ for all clauses.

The proof is in the Appendix D. As for a single clause, we set the total LagONN dynamics to reach a saddle point as:

$$\begin{cases} \tau \dot{\phi}_x = -\nabla_{\phi_x} L_T = -\sum_m u_\lambda^m \cdot \partial \vec{Z}_m / \partial \phi_x \\ \tau_\lambda \dot{\phi}_\lambda = +\nabla_{\phi_\lambda} L_T = \sum_m u_\lambda^m \cdot \vec{Z}_m \end{cases} \quad (16)$$

Fig.4a and b show examples of phase dynamics without and with Lagrange oscillators for $N = 20$ variables and $M = 91$ clauses (satisfiable instance cnf-20-01 from SATlib [38]). The ONN phases settle to non-binary values and

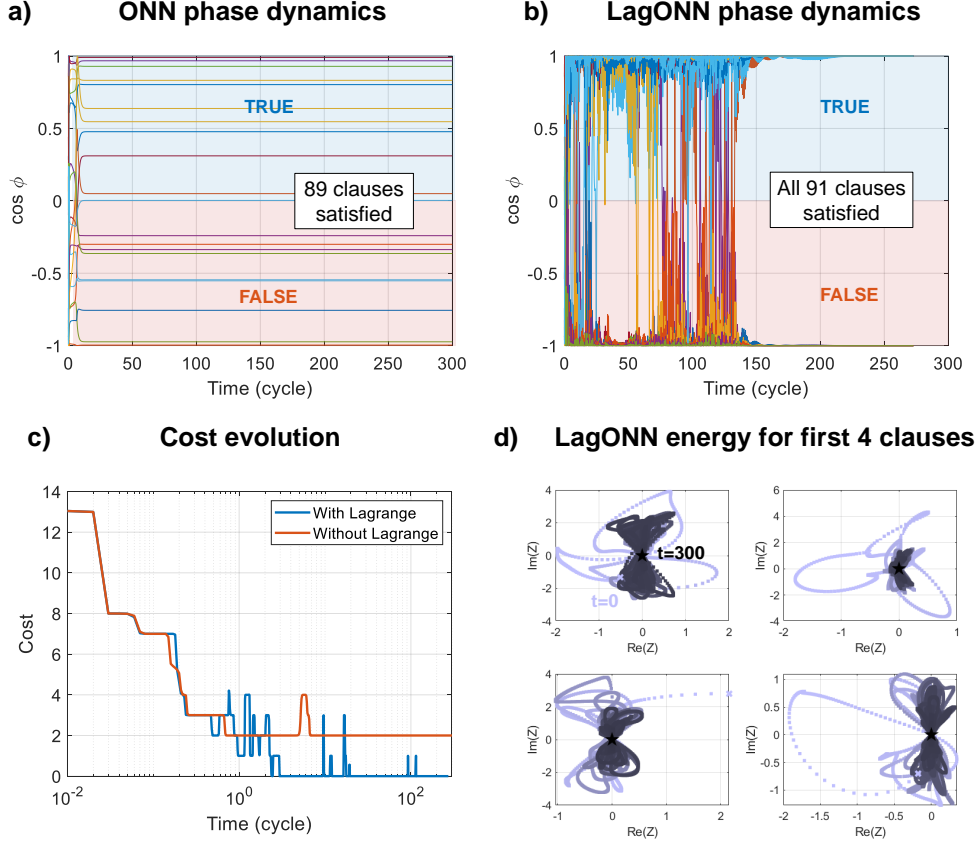


Figure 4: Phase dynamics for the satisfiable SATlib instance 'cnf-20-01' with $N = 20$ variables and $M = 91$ clauses. a) Standard ONN dynamics quickly converge toward a sub-optimal solution where 89/91 of clauses are satisfied. b) With the same initialization, the Lagrange version takes more time to reach a fixed point. Reading out the phases gives an optimal Boolean assignment where all clauses are satisfied. c) Cost function comparison between the two approaches. LagONN finds an assignment of optimal phase around the same time the standard ONN settles (≈ 10 oscillation cycles). By measuring the cost in real time, we can stop the run when a target cost is reached without waiting for convergence. d) Dynamics for four LagONN energy terms Z_m corresponding to the first four clauses. While the dynamics almost seem chaotic, they evolve to reach a target saddle point where all $Z_m = 0$. Eventually, the dynamics converge toward a fixed point at $t=300$ oscillation cycles where all $Z_m = 0$.

we round the phases to the closest multiple of π to obtain the corresponding Boolean values and compute the cost. This leads to a sub-optimal solution where 2 clauses remain unsatisfied. With Lagrange oscillators, we notice that the dynamics are much more complex and take longer to settle. However, phases settle to multiples of π , which removes the need to round and provides an optimal Boolean assignment where all 91 clauses are satisfied. Informally, we believe the system frustration occurring with many clauses reduces the saddle points to binary phases only. Fig.4d shows the dynamics of the first four energy terms Z_m that are simultaneously attracted by the origin $Z_m = 0$ corresponding to a target saddle point. An optimal assignment is found when all Z_m trajectories reach $Z_m = 0$. Fig.4c compares the cost function evolution for the two cases. Interestingly, LagONN dynamics reduce the cost as fast as the ONN case, and after one oscillation cycle, it reaches the same cost of around 2 unsatisfied clauses. A couple of oscillations after, LagONN dynamics do not get stuck but rather find an optimal Boolean assignment. Comparing the phase dynamics from Fig.4b with the cost evolution in Fig.4c, it is clear that some phases continue to evolve with minimal impact on the cost. Hence, for all the simulations in this paper, we monitor the cost in real-time and stop the simulation when the cost reaches a satisfactory value (set to 0 for satisfiable instances), as discussed in the Appendix A. In other words, we do not wait until the convergence towards an optimal saddle point as in Fig.4b, whose stability is not guaranteed under the flow given by Eq. 13 and requires further analysis.

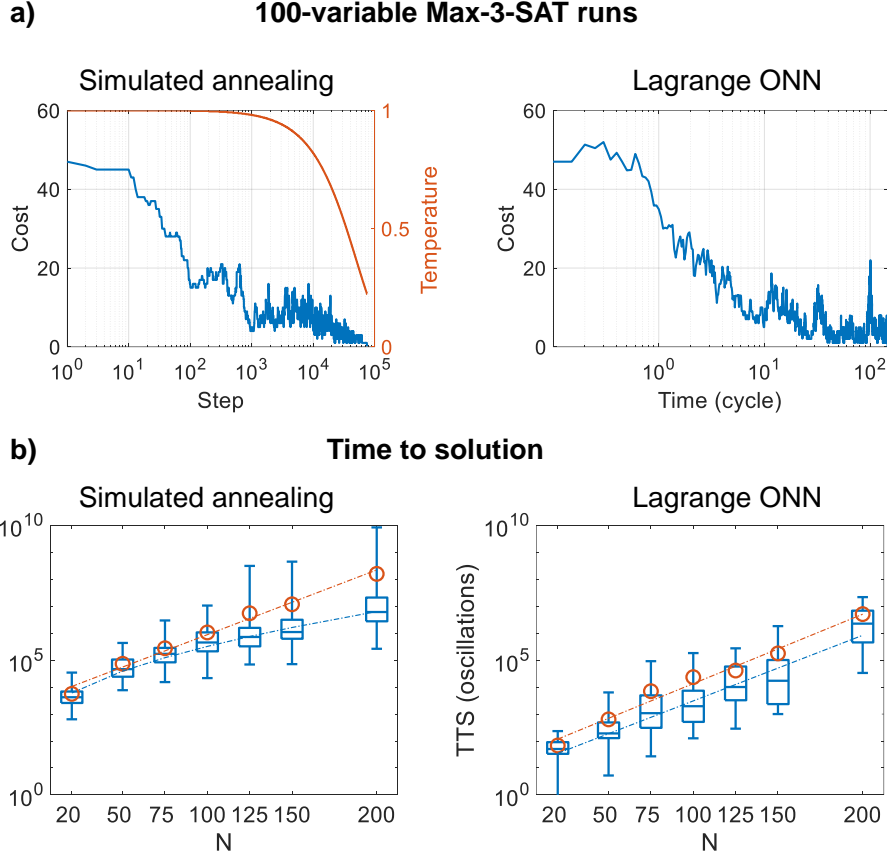


Figure 5: a) Cost evolution comparison for a SATlib instance with 100 variables and 430 clauses, where all variables are initialized to '1'. The temperature in simulated annealing decreases exponentially with the number of steps as described in the Appendix C. b) Estimation of the time to reach an optimal solution with 99% probability. It is defined as $t_{max} \times \log(0.01)/\log(1 - p_s)$ where t_{max} is the maximum simulation time and p_s is the corresponding success probability. Boxes show the 1st, 2nd, and 3rd quartiles computed for the first 30 satisfiable instances from SATlib for LagONN, and 100 instances for simulated annealing. The error bars show the min-max values, and red circles are the averages. For both simulated annealing and LagONN methods, we increase t_{max} with the size to get at least one optimal solution among 100 trials for each instance. For both methods, we fit the logarithm of data to estimate the mean TTS scaling as $\sim \exp(aN + b)$ with $a = 0.059$, $b = 3.58$ for LagONN and $a = 0.055$, $b = 8.16$ for simulated annealing (red dashed lines). Simulated annealing has an advantageous scaling for the median TTS fitted as $\sim \exp(c\sqrt{N} + d)$ with $c = 0.719$, $d = 5.49$, whereas we fit LagONN's median TTS as $\sim \exp(aN + b)$ with $a = 0.056$ and $b = 2.43$ (blue dashed curves).

3.4 Comparison with simulated annealing and time to solution

We compare LagONN's search with a simulated annealing algorithm for SAT [66] detailed in the Appendix C. Each SAT variable is sequentially flipped and the corresponding cost change δ is calculated. A flip is accepted with probability $1/(1 + \exp(\delta/T))$ where T is a temperature parameter. During the execution, the temperature exponentially decreases from T_{max} to T_{min} to anneal the system and reach low-cost values. We set $T_{max} = 1$ and $T_{min} = 0.01$ found empirically by inspecting the cost evolution for various sizes. We use an exponential schedule as proposed in [66], providing satisfactory results but we do not claim optimality. An example of simulated annealing run is shown in Fig.5a (left) for 100 variables and 430 clauses where the x-axis corresponds to the number of steps (tentative flips). In this example, the 100 variables are initialized to '1'. After the first 100 steps of the algorithm execution (a sweep), every variable has been considered and flipped according to the sigmoid probability at $T = T_{max}$. At this temperature, the variable sweep induces a steep cost reduction of around 30 satisfied clauses. Then, the algorithm enters a regime with fewer variable flips and the average cost slowly decreases with the temperature. We stop the algorithm when it finds

Table 2: Comparison between simulated annealing and Lagrange ONN for solving the Max-3-SAT constraint satisfaction problem from both conceptual and practical (hardware) points of view.

	Simulated annealing	Lagrange ONN
Strengths	Advantageous TTS scaling. Convergence at cold temperature.	Noiseless approach. Cannot settle into infeasible states.
Weaknesses	Requires careful noise tuning. Can be stuck at infeasible states.	Seemingly worse TTS scaling. Stability is not guaranteed.

an optimal variable assignment. A LagONN simulation is shown in Fig.5a (right) for the same variable initialization and a random Lagrange oscillator initialization. The LagONN cost evolution is qualitatively different from simulated annealing as LagONN does not have any annealing mechanism and continues to make uphill moves at low-cost values, which is very unlikely for simulated annealing at low temperature. The major difference is that LagONN dynamics do not stop until the constraints are met, unlike simulated annealing which can freeze to a non-optimal state for a finite annealing time. However, this does not mean that LagONN’s search is more efficient, as we show next by comparing the time to solution between the two algorithms.

Now, we assess the performances of LagONN and simulated annealing on hard random instances from SATlib [38] with increasing sizes $(N, M) \in \{(20, 91), (50, 218), (75, 325), (100, 430), (125, 538), (150, 645), (200, 860)\}$. This is a notoriously difficult benchmark as the instances are close to criticality where $M \approx 4.3N$ [67]. For each (N, M) from the library, we select the first 100 and 30 instances for simulated annealing and LagONN (fewer instances due to very long LagONN simulation time). Then, we run 100 transient simulations per instance with random initial phase values sampled uniformly, and fixed runtime t_{max} to estimate a corresponding success probability p_s . The metric generally used for Ising machines is the time to solution (TTS) that expresses the time for the system to reach an optimal solution with some probability, often set to 0.99. The TTS is then calculated for each instance as:

$$TTS = t_{max} \frac{\log(0.01)}{\log(1 - p_s)} \quad (17)$$

We use the same TTS formula for simulated annealing with $t_{max} = n_{max}$ representing the number of fixed algorithmic steps per run (maximum number of variable updates). When assessing the TTS scaling with the system size, the runtime needs to be optimized for every size to avoid wrong scaling assessments such as flat curve effects occurring when t_{max} is too large, or overestimation of TTS when t_{max} is too small at a large size [68]. Hence, we iteratively increase t_{max} and n_{max} with the size up to $t_{max} \leq 10^6$ oscillation cycles, and $n_{max} \leq 2 \times 10^7$ steps to keep p_s in the range $0.1 < p_s < 0.9$ for all instances.

Fig.5b shows the TTS scaling with size in a semilog plot, with blue boxes corresponding to 1st, 2nd, and 3rd quartiles. Qualitatively, simulated annealing seems to have an advantageous scaling compared to LagONN on this benchmark, as the slope flattens at larger sizes. In particular, we fit the median TTS as $\sim \exp(c\sqrt{N} + d)$ with $c = 0.719$, $d = 5.49$, whereas LagONN’s median TTS shows a straight line in semilog plot, fitted as $\sim \exp(aN + b)$ with $a = 0.056$ and $b = 2.43$ (blue dashed curves). Note that for simulated annealing, we dismissed a polynomial scaling for the median TTS as we did not observe a straight line in a log-log plot. At large sizes, LagONN’s TTS has fewer outliers than simulated annealing, with a mean TTS scaling similarly to median values as $\sim \exp(aN + b)$ with $a = 0.059$, $b = 3.58$. In contrast, simulated annealing sometimes suffers from very hard instances and has more than 5 decades of variations at $N = 200$, inducing a scaling slope for the mean values similar to LagONN as $\sim \exp(aN + b)$ with $a = 0.055$, $b = 8.16$. Although simulated annealing seems better suited for this benchmark due to an advantageous scaling for the median TTS, LagONN’s TTS benefits from a lower prefactor $\exp(2.43) < \exp(5.49)$ which keeps it competitive for $N \leq 200$. We remain cautious about our TTS scaling estimation since we used a limited number of instances and sizes due to very long simulation times (see Appendix B). Nevertheless, the results confirm LagONN’s ability to enforce constraint satisfaction by escaping infeasible states in a deterministic manner. As such, similar competitive dynamics for coupled oscillators could solve constrained optimization problems expressed with a Lagrange function (Eq. 5), as we discuss next with the example of phase buffering.

4 Summary and Discussion

In this paper, we showed how using additional Lagrange oscillators in coupled oscillator systems can enforce constraint satisfaction, such as solving Max-3-SAT problems. These problems are particular cases where the Lagrange function only consists of the constraint function g that counts the number of unsatisfied clauses (no additional cost function f). Since the Lagrange oscillators do not stop until the constraints are satisfied, LagONN searches the space until it finds an optimal solution, an advantage compared to simulated annealing, which can get stuck in local minima. Moreover,

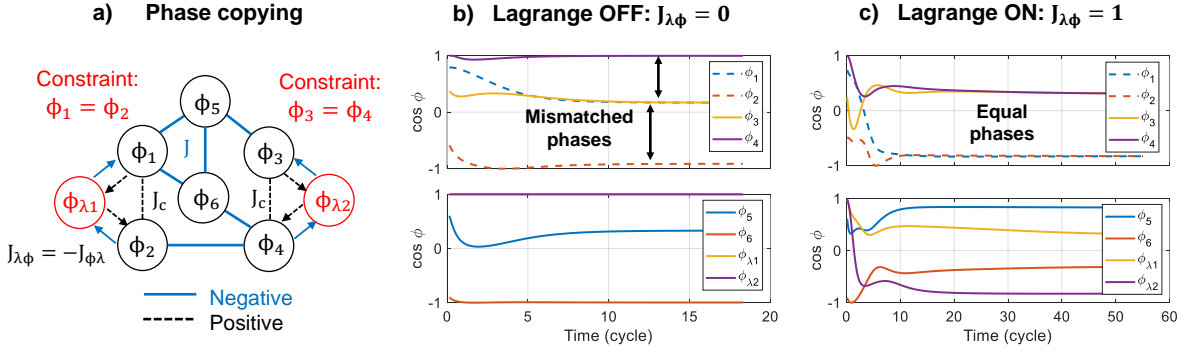


Figure 6: LagONN for phase copying on an initial graph with negative coupling $J = -1$ (blue edge). a) In practice at a large scale, Ising machines often have limited hardware connectivity, and dense graphs are mapped to a sparser network by introducing copy nodes [69]. Ideally, the copy nodes should copy the original values, e.g. $\cos \phi_2 = \cos \phi_1$. This is generally achieved with a ferromagnetic coupling between the two nodes ($J_c = +0.5$ here). Ideally, the positive coupling should be large enough to keep the two variables identical. However, a large coupling value introduces rigidity in the system, and finding the ground states of the original problem becomes very challenging. b) For weak coupling values such as in this example, the copied phases are not identical ($\cos \phi_1 \neq \cos \phi_2$). c) Lagrange oscillators can enforce the copy constraints between two copied nodes, as shown in this example for $J_{\lambda\phi} = 1$.

LagONN is a noiseless method and does not require annealing. This is particularly interesting for coupled oscillators, as tuning noise in a physical implementation can be challenging. However, LagONN's search for optimal Boolean assignments seems less effective than simulated annealing, as suggested by our time-to-solution study. Moreover, the stability of the saddle points reached by the dynamics defined in Eq. 16 is not guaranteed and requires further analysis. The strengths and weaknesses of each method are summarized in Table 2.

Beyond pure constraint satisfaction problems, LagONN can be useful for more general constrained problems with both a cost f and constraints g . For instance, Fig.6 presents the problem of phase copying that would occur on hardware at a large scale. Suppose a large problem represented as a dense graph cannot be implemented due to the quadratic number of edges. In that case, one has to introduce copy nodes that *copy* each other to distribute the edges among them [69]. This is a typical constraint for quantum annealers that have a limited connectivity [70]. The constraint function g then expresses the equality requirement between copies, whereas the cost function f is the Ising energy corresponding to the original graph. To copy the spin values, we can intuitively set a ferromagnetic coupling J_c between the two nodes, corresponding to the penalty method expressed for copy constraints as $\frac{J_c}{2}(S_1 - S_2)^2 \equiv -J_c S_1 S_2$. Ideally, this positive coupling should be sufficiently large to meet the constraint. However, in practice, it has been shown that the coupling strength cannot be too large at the risk of rigidifying the dynamics and challenging the search for energy ground states [7, 69].

Fig.6a shows an example of a coupled oscillator network with coupling $J = -1$ (blue edges) and copy coupling J_c (dashed black edges). The cost function f to minimize is the XY Ising energy E for phase oscillators (Eq. 3) determined by the symmetric couplings. Here the copy constraints are $g = (\cos \phi_1 - \cos \phi_2, \cos \phi_3 - \cos \phi_4) = 0$. When the constraints are met, the graph reduces to a 4-node fully-connected graph. Fig.6b shows an example of phase dynamics with a weak copy coupling $J_c = +0.5$ where the phases are not identical, e.g. $\cos \phi_1 \neq \cos \phi_2$.

Instead of increasing J_c at the risk of rigidifying the system, one can introduce a Lagrange oscillator per constraint to maintain the phases identical as shown in Fig.6c. Taking the example of ϕ_1 and ϕ_2 , the corresponding copy constraint can be expressed as a vector $Z_{1-2}^{\rightarrow} = \exp(i\phi_1) - \exp(i\phi_2) = 0$. Similarly to how we defined the Lagrange function for 3-SAT (Eq. 15), the corresponding Lagrange term for this constraint is expressed as:

$$u_{\lambda 1}^{\rightarrow} \cdot Z_{1-2}^{\rightarrow} = \cos(\phi_1 - \phi_{\lambda 1}) - \cos(\phi_2 - \phi_{\lambda 1}) \quad (18)$$

where $\phi_{\lambda 1}$ is the phase of the Lagrange oscillator connected to the first two oscillators. The total Lagrange function for this example is then:

$$L(\phi, \phi_{\lambda}) = E(\phi) + J_{\lambda\phi} (u_{\lambda 1}^{\rightarrow} \cdot Z_{1-2}^{\rightarrow} + u_{\lambda 2}^{\rightarrow} \cdot Z_{3-4}^{\rightarrow}) \quad (19)$$

where $J_{\lambda\phi}$ sets the constraint strength or equivalently, the speed of Lagrange oscillators. Setting competitive dynamics seeking a saddle point in the Lagrange landscape as Eq. 16, ϕ_{λ} performs gradient ascent until the constraints are

satisfied, while other phases ϕ do gradient descent to minimize L . Note that these opposite signs in the gradient induce asymmetric couplings between oscillators and Lagrange oscillators, as highlighted by the arrows in Fig.6a with weights set to $J_{\lambda\phi} = -J_{\phi\lambda} = 1$. The main drawback of this approach is that the stability of fixed points is not guaranteed and requires further analytical investigation. For instance, we find in simulations that increasing the strength $J_{\lambda\phi}$ speeds up the Lagrange oscillators and introduces transient and decaying phase oscillations. In contrast, increasing the copying strength J_c acts as an increasing damping factor and smooths out the dynamics. Such a combination of energy penalties (set by J_c) and Lagrange multipliers could augment existing oscillatory Ising machines, as proposed in previous work and resulting in orders of magnitude speed up compared to fixed energy penalties for knapsack problems [71]. The analysis of these different regimes is left as future work.

5 Conclusion

This article introduced LagONN, a Lagrange oscillatory neural network that enforces constraint satisfaction as demonstrated for the Max-3-SAT problem. Compared to gradient-descent-based approaches such as oscillatory Ising machines that can get stuck at infeasible local minima, LagONN employs additional Lagrange oscillators that force 3-SAT clauses to be satisfied. Conceptually, these new Lagrange variables offer alternative paths in the energy landscape to escape local minima and reach optimal states where phases correspond to optimal Boolean values. When benchmarked on SATlib instances up to 200 variables and 860 clauses against simulated annealing, LagONN simulations showed a seemingly less favorable time-to-solution scaling with increasing problem size, although remaining competitive for the tested problem sizes ($N \leq 200$) due to a smaller prefactor in the scaling function. Specifically, for the Max-3-SAT constraint satisfaction problem, LagONN offers an alternative deterministic search method and removes the need for careful noise control in simulated annealing, which can be difficult to implement in hardware. Moreover, with the example of phase copying, we showed that oscillatory-based Ising machines combined with Lagrange oscillators could enforce constraint satisfaction in optimization, beyond the penalty method.

Declarations

This work was supported by the European Union’s Horizon 2020 research and innovation program, EU H2020 NEURONN (www.neuronn.eu) project under Grant 871501. BM, FS, and ATS acknowledge support from the European Union’s Horizon Europe research and innovation programme, PHASTRAC project under grant agreement No 101092096 and Dutch Research Council’s AiNed Fellowship research programme, AI-on-ONN project under grant agreement No. NGF.1607.22.016, as well as funding from the European Research Council ERC THERMODON project under grant agreement No. 101125031.

Code availability

Matlab codes are available at the following GitHub repository:

<https://github.com/corentindelacour/Lagrange-oscillatory-neural-network>

References

- [1] Stephen A. Cook. The complexity of theorem-proving procedures. In *Proceedings of the Third Annual ACM Symposium on Theory of Computing*, STOC ’71, page 151–158, New York, NY, USA, 1971. Association for Computing Machinery.
- [2] Naeimeh Mohseni, Peter L. McMahon, and Tim Byrnes. Ising machines as hardware solvers of combinatorial optimization problems. *Nature Reviews Physics*, 4(6):363–379, Jun 2022.
- [3] J J Hopfield. Neural networks and physical systems with emergent collective computational abilities. *Proceedings of the National Academy of Sciences*, 79(8):2554–2558, 1982.
- [4] D. Tank and J. Hopfield. Simple ’neural’ optimization networks: An A/D converter, signal decision circuit, and a linear programming circuit. *IEEE Transactions on Circuits and Systems*, 33(5):533–541, May 1986.
- [5] J J Hopfield. Neurons with graded response have collective computational properties like those of two-state neurons. *Proceedings of the National Academy of Sciences*, 81(10):3088–3092, May 1984.
- [6] Andrew Lucas. Ising formulations of many NP problems. *Frontiers in Physics*, 2, 2014.

- [7] Davide Venturelli, Salvatore Mandrà, Sergey Knysh, Bryan O’Gorman, Rupak Biswas, and Vadim Smelyanskiy. Quantum optimization of fully connected spin glasses. *Phys. Rev. X*, 5:031040, Sep 2015.
- [8] Matthieu Parizy and Nozomu Togawa. Analysis and Acceleration of the Quadratic Knapsack Problem on an Ising Machine. *IEICE Transactions on Fundamentals of Electronics, Communications and Computer Sciences*, E104.A(11):1526–1535, November 2021.
- [9] Lorenzo Cellini, Antonio Macaluso, and Michele Lombardi. QAL-BP: an augmented Lagrangian quantum approach for bin packing. *Scientific Reports*, 14(1):5142, March 2024.
- [10] Magnus R. Hestenes. Multiplier and gradient methods. *Journal of Optimization Theory and Applications*, 4(5):303–320, November 1969.
- [11] M. J. D. Powell. Algorithms for nonlinear constraints that use lagrangian functions. *Mathematical Programming*, 14(1):224–248, December 1978.
- [12] Sri Krishna Vadlamani, Tianyao Patrick Xiao, and Eli Yablonovitch. Physics successfully implements Lagrange multiplier optimization. *Proceedings of the National Academy of Sciences*, 117(43):26639–26650, October 2020.
- [13] M. Nagamatu and T. Yanaru. On the stability of lagrange programming neural networks for satisfiability problems of propositional calculus. *Neurocomputing*, 13(2):119–133, 1996. Soft Computing.
- [14] S. Kirkpatrick, C. D. Gelatt, and M. P. Vecchi. Optimization by simulated annealing. *Science*, 220(4598):671–680, 1983.
- [15] Aida Todri-Sanial, Corentin Delacour, Madeleine Abernot, and Filip Sabo. Computing with oscillators from theoretical underpinnings to applications and demonstrators. *npj Unconventional Computing*, 1(1):14, Dec 2024.
- [16] Abhinav Parihar, Nikhil Shukla, Matthew Jerry, Suman Datta, and Arijit Raychowdhury. Vertex coloring of graphs via phase dynamics of coupled oscillatory networks. *Scientific Reports*, 7(1):911, Apr 2017.
- [17] Tianshi Wang, Leon Wu, Parth Nobel, and Jaijeet Roychowdhury. Solving combinatorial optimisation problems using oscillator based ising machines. *Natural Computing*, 20(2):287–306, Jun 2021.
- [18] Markus Graber and Klaus Hofmann. A versatile and adjustable 400 node cmos oscillator based ising machine to investigate and optimize the internal computing principle. In *2022 IEEE 35th International System-on-Chip Conference (SOCC)*, pages 1–6, 2022.
- [19] Markus Graber and Klaus Hofmann. A Coupled Oscillator Network to Solve Combinatorial Optimization Problems with Over 95% Accuracy. In *2023 IEEE International Symposium on Circuits and Systems (ISCAS)*, pages 1–5, Monterey, CA, USA, May 2023. IEEE.
- [20] Corentin Delacour, Stefania Carapezzi, Gabriele Boschetto, Madeleine Abernot, Thierry Gil, Nadine Azemard, and Aida Todri-Sanial. A mixed-signal oscillatory neural network for scalable analog computations in phase domain. *Neuromorphic Computing and Engineering*, 3(3):034004, aug 2023.
- [21] Mohammad Khairul Bashar and Nikhil Shukla. Designing Ising machines with higher order spin interactions and their application in solving combinatorial optimization. *Scientific Reports*, 13(1):9558, June 2023.
- [22] Antik Mallick, Mohammad Khairul Bashar, Daniel S. Truesdell, Benton H. Calhoun, Siddharth Joshi, and Nikhil Shukla. Using synchronized oscillators to compute the maximum independent set. *Nature Communications*, 11(1):4689, Sep 2020.
- [23] Ibrahim Ahmed, Po-Wei Chiu, William Moy, and Chris H. Kim. A probabilistic compute fabric based on coupled ring oscillators for solving combinatorial optimization problems. *IEEE Journal of Solid-State Circuits*, 56(9):2870–2880, 2021.
- [24] William Moy, Ibrahim Ahmed, Po-wei Chiu, John Moy, Sachin S. Sapatnekar, and Chris H. Kim. A 1,968-node coupled ring oscillator circuit for combinatorial optimization problem solving. *Nature Electronics*, 5(5):310–317, May 2022.
- [25] Markus Graber and Klaus Hofmann. An integrated coupled oscillator network to solve optimization problems. *Communications Engineering*, 3(1):116, Aug 2024.
- [26] J. Grollier, D. Querlioz, K. Y. Camsari, K. Everschor-Sitte, S. Fukami, and M. D. Stiles. Neuromorphic spintronics. *Nature Electronics*, 3(7):360–370, Jul 2020.
- [27] Andrea Grimaldi, Luciano Mazza, Eleonora Raimondo, Pietro Tullo, Davi Rodrigues, Kerem Y. Camsari, Vincenza Crupi, Mario Carpentieri, Vito Puliafito, and Giovanni Finocchio. Evaluating spintronics-compatible implementations of ising machines. *Phys. Rev. Appl.*, 20:024005, Aug 2023.

- [28] S. Dutta, A. Khanna, A. S. Assoa, H. Paik, D. G. Schlom, Z. Toroczkai, A. Raychowdhury, and S. Datta. An ising hamiltonian solver based on coupled stochastic phase-transition nano-oscillators. *Nature Electronics*, 4(7):502–512, Jul 2021.
- [29] Hyun Wook Kim, Seonuk Jeon, Heebum Kang, Eunryeong Hong, Nayeon Kim, and Jiyong Woo. Understanding rhythmic synchronization of oscillatory neural networks based on nbox artificial neurons for edge detection. *IEEE Transactions on Electron Devices*, 70(6):3031–3036, 2023.
- [30] Olivier Maher, Manuel Jiménez, Corentin Delacour, Nele Harnack, Juan Núñez, María J. Avedillo, Bernabé Linares-Barranco, Aida Todri-Sanial, Giacomo Indiveri, and Siegfried Karg. A cmos-compatible oscillation-based vo2 ising machine solver. *Nature Communications*, 15(1):3334, Apr 2024.
- [31] Seong-Yun Yun, Joon-Kyu Han, and Yang-Kyu Choi. A nanoscale bistable resistor for an oscillatory neural network. *Nano Letters*, 24(9):2751–2757, Mar 2024.
- [32] Anshujit Sharma, Matthew Burns, Andrew Hahn, and Michael Huang. Augmenting an electronic ising machine to effectively solve boolean satisfiability. *Scientific Reports*, 13(1):22858, Dec 2023.
- [33] Yuqi Su, Tony Tae-Hyoung Kim, and Bongjin Kim. A reconfigurable Ising machine for boolean satisfiability problems featuring many-body spin interactions. In *2023 IEEE Custom Integrated Circuits Conference (CICC)*, pages 1–2, 2023.
- [34] Mohammad Hizzani, Arne Heitmann, George Hutchinson, Dmitri Dobrynin, Thomas Van Vaerenbergh, Tinish Bhattacharya, Adrien Renaudineau, Dmitri Strukov, and John Paul Strachan. Memristor-based hardware and algorithms for higher-order hopfield optimization solver outperforming quadratic ising machines. In *2024 IEEE International Symposium on Circuits and Systems (ISCAS)*, pages 1–5, 2024.
- [35] Giacomo Pedretti, Fabian Böhm, Tinish Bhattacharya, Arne Heitmann, Xiangyi Zhang, Mohammad Hizzani, George Hutchinson, Dongseok Kwon, John Moon, Elisabetta Valiante, Ignacio Rozada, Catherine E. Graves, Jim Ignowski, Masoud Mohseni, John Paul Strachan, Dmitri Strukov, Ray Beausoleil, and Thomas Van Vaerenbergh. Solving boolean satisfiability problems with resistive content addressable memories. *npj Unconventional Computing*, 2(1):7, Apr 2025.
- [36] Evangelos Dikopoulos, Ying-Tuan Hsu, Luke Wormald, Wei Tang, Zhengya Zhang, and Michael P. Flynn. 25.1 a physics-inspired oscillator-based mixed-signal optimization engine for solving 50-variable 218-clause 3-sat problems with 100In 2025 *IEEE International Solid-State Circuits Conference (ISSCC)*, volume 68, pages 01–03, 2025.
- [37] Ahmet Yusuf Salim, Bart Selman, Henry Kautz, Zeljko Ignjatovic, and Selçuk Köse. Ski-sat: A cmos-compatible hardware for solving sat problems. *IEEE Transactions on Circuits and Systems I: Regular Papers*, pages 1–12, 2025.
- [38] Holger Hoos. Satlib - benchmark problems. <https://www.cs.ubc.ca/~hoos/SATLIB/benchm.html>, 2000. [Online; accessed 13-October 2023].
- [39] Kerem Yunus Camsari, Rafatul Faria, Brian M. Sutton, and Supriyo Datta. Stochastic p -bits for invertible logic. *Phys. Rev. X*, 7:031014, Jul 2017.
- [40] Fuxi Cai, Suhas Kumar, Thomas Van Vaerenbergh, Xia Sheng, Rui Liu, Can Li, Zhan Liu, Martin Foltin, Shimeng Yu, Qiangfei Xia, J. Joshua Yang, Raymond Beausoleil, Wei D. Lu, and John Paul Strachan. Power-efficient combinatorial optimization using intrinsic noise in memristor hopfield neural networks. *Nature Electronics*, 3(7):409–418, Jul 2020.
- [41] Shuvro Chowdhury, Andrea Grimaldi, Navid Anjum Aadit, Shaila Niazi, Masoud Mohseni, Shun Kanai, Hideo Ohno, Shunsuke Fukami, Luke Theogarajan, Giovanni Finocchio, Supriyo Datta, and Kerem Y. Camsari. A full-stack view of probabilistic computing with p-bits: Devices, architectures, and algorithms. *IEEE Journal on Exploratory Solid-State Computational Devices and Circuits*, 9(1):1–11, 2023.
- [42] Nihal Sanjay Singh, Keito Kobayashi, Qixuan Cao, Kemal Selcuk, Tianrui Hu, Shaila Niazi, Navid Anjum Aadit, Shun Kanai, Hideo Ohno, Shunsuke Fukami, and Kerem Y. Camsari. Cmos plus stochastic nanomagnets enabling heterogeneous computers for probabilistic inference and learning. *Nature Communications*, 15(1):2685, Mar 2024.
- [43] Navid Anjum Aadit, Andrea Grimaldi, Mario Carpentieri, Luke Theogarajan, John M. Martinis, Giovanni Finocchio, and Kerem Y. Camsari. Massively Parallel Probabilistic Computing with Sparse Ising Machines. *Nature Electronics*, 5(7):460–468, June 2022. arXiv:2110.02481 [cond-mat].
- [44] Emile Aarts and Jan Korst. *Simulated annealing and Boltzmann machines: a stochastic approach to combinatorial optimization and neural computing*. John Wiley & Sons, Inc., USA, 1989.

- [45] Z. Fahimi, M. R. Mahmoodi, H. Nili, Valentin Polishchuk, and D. B. Strukov. Combinatorial optimization by weight annealing in memristive hopfield networks. *Scientific Reports*, 11(1):16383, August 2021.
- [46] Mingrui Jiang, Keyi Shan, Chengping He, and Can Li. Efficient combinatorial optimization by quantum-inspired parallel annealing in analogue memristor crossbar. *Nature Communications*, 14(1):5927, September 2023.
- [47] Mária Ercsey-Ravasz and Zoltán Toroczkai. Optimization hardness as transient chaos in an analog approach to constraint satisfaction. *Nature Physics*, 7(12):966–970, December 2011.
- [48] Botond Molnár and Mária Ercsey-Ravasz. Asymmetric Continuous-Time Neural Networks without Local Traps for Solving Constraint Satisfaction Problems. *PLoS ONE*, 8(9):e73400, September 2013.
- [49] Fabio L. Traversa and Massimiliano Di Ventra. Polynomial-time solution of prime factorization and NP-complete problems with digital memcomputing machines. *Chaos: An Interdisciplinary Journal of Nonlinear Science*, 27(2):023107, February 2017.
- [50] Hayato Goto, Kosuke Tatsumura, and Alexander R. Dixon. Combinatorial optimization by simulating adiabatic bifurcations in nonlinear Hamiltonian systems. *Science Advances*, 5(4):eaav2372, April 2019.
- [51] Hideyuki Suzuki, Jun-ichi Imura, Yoshihiko Horio, and Kazuyuki Aihara. Chaotic boltzmann machines. *Scientific Reports*, 3(1):1610, Apr 2013.
- [52] Kyle Lee, Shuvro Chowdhury, and Kerem Y. Camsari. Noise-augmented chaotic ising machines for combinatorial optimization and sampling. *Communications Physics*, 8(1):35, Jan 2025.
- [53] Botond Molnár, Ferenc Molnár, Melinda Varga, Zoltán Toroczkai, and Mária Ercsey-Ravasz. A continuous-time MaxSAT solver with high analog performance. *Nature Communications*, 9(1):4864, November 2018.
- [54] E.M. Izhikevich and Y. Kuramoto. Weakly coupled oscillators. In *Encyclopedia of Mathematical Physics*, pages 448–453. Academic Press, 2006.
- [55] T. Jackson, S. Pagliarini, and L. Pileggi. An oscillatory neural network with programmable resistive synapses in 28 nm cmos. In *2018 IEEE International Conference on Rebooting Computing (ICRC)*, pages 1–7, 2018.
- [56] Madeleine Abernot, Thierry Gil, Manuel Jiménez, Juan Núñez, María J. Avellido, Bernabé Linares-Barranco, Théophile Gonos, Tanguy Hardelin, and Aida Todri-Sanial. Digital implementation of oscillatory neural network for image recognition applications. *Frontiers in Neuroscience*, 15:1095, 2021.
- [57] Tianshi Wang, Leon Wu, and Jaijeet Roychowdhury. New computational results and hardware prototypes for oscillator-based ising machines. In *Proceedings of the 56th Annual Design Automation Conference 2019, DAC '19*, New York, NY, USA, 2019. Association for Computing Machinery.
- [58] Samuel Burer, Renato Monteiro, and Yin Zhang. Rank-two relaxation heuristics for max-cut and other binary quadratic programs. *SIAM Journal on Optimization*, 12, 07 2001.
- [59] Mikhail Erementchouk, Aditya Shukla, and Pinaki Mazumder. On computational capabilities of ising machines based on nonlinear oscillators. *Physica D: Nonlinear Phenomena*, 437:133334, 2022.
- [60] Connor Bybee, Denis Kleyko, Dmitri E. Nikonov, Amir Khosrowshahi, Bruno A. Olshausen, and Friedrich T. Sommer. Efficient optimization with higher-order ising machines. *Nature Communications*, 14(1):6033, September 2023.
- [61] Marshall L. Fisher. The Lagrangian Relaxation Method for Solving Integer Programming Problems. *Management Science*, 50(12):1861–1871, 2004.
- [62] Benjamin W. Wah and Zhe Wu. The Theory of Discrete Lagrange Multipliers for Nonlinear Discrete Optimization. In Gerhard Goos, Juris Hartmanis, Jan Van Leeuwen, and Joxan Jaffar, editors, *Principles and Practice of Constraint Programming – CP'99*, volume 1713, pages 28–42. Springer Berlin Heidelberg, Berlin, Heidelberg, 1999. Series Title: Lecture Notes in Computer Science.
- [63] Stephen P. Boyd and Lieven Vandenbergh. *Convex optimization*. Cambridge University Press, Cambridge New York Melbourne New Delhi Singapore, version 29 edition, 2023.
- [64] S. Zhang and A.G. Constantinides. Lagrange programming neural networks. *IEEE Transactions on Circuits and Systems II: Analog and Digital Signal Processing*, 39(7):441–452, July 1992.
- [65] Elisabetta Corti, Joaquin Antonio Cornejo Jimenez, Kham M. Niang, John Robertson, Kirsten E. Moselund, Bernd Gotsmann, Adrian M. Ionescu, and Siegfried Karg. Coupled vo2 oscillators circuit as analog first layer filter in convolutional neural networks. *Frontiers in Neuroscience*, 15:19, 2021.
- [66] David Johnson and Michael Trick, editors. *Cliques, Coloring, and Satisfiability*, volume 26 of *DIMACS Series in Discrete Mathematics and Theoretical Computer Science*. American Mathematical Society, Providence, Rhode Island, October 1996.

- [67] David Mitchell, Bart Selman, and Hector Levesque. Hard and easy distributions of sat problems. In *Proceedings of the Tenth National Conference on Artificial Intelligence, AAAI'92*, page 459–465. AAAI Press, 1992.
- [68] Troels F. Rønnow, Zhihui Wang, Joshua Job, Sergio Boixo, Sergei V. Isakov, David Wecker, John M. Martinis, Daniel A. Lidar, and Matthias Troyer. Defining and detecting quantum speedup. *Science*, 345(6195):420–424, 2014.
- [69] M Mahmudul Hasan Sajeeb, Navid Anjum Aadit, Shuvro Chowdhury, Tong Wu, Cesely Smith, Dhruv Chinmay, Atharva Raut, Kerem Y. Camsari, Corentin Delacour, and Tathagata Srimani. Scalable connectivity for ising machines: Dense to sparse. *arXiv:2503.01177*, 2025.
- [70] Elijah Pelofske. Comparing three generations of d-wave quantum annealers for minor embedded combinatorial optimization problems. *Quantum Science and Technology*, 10, 02 2025.
- [71] Corentin Delacour. Self-adaptive ising machines for constrained optimization. *arXiv:2501.04971*, 2025.

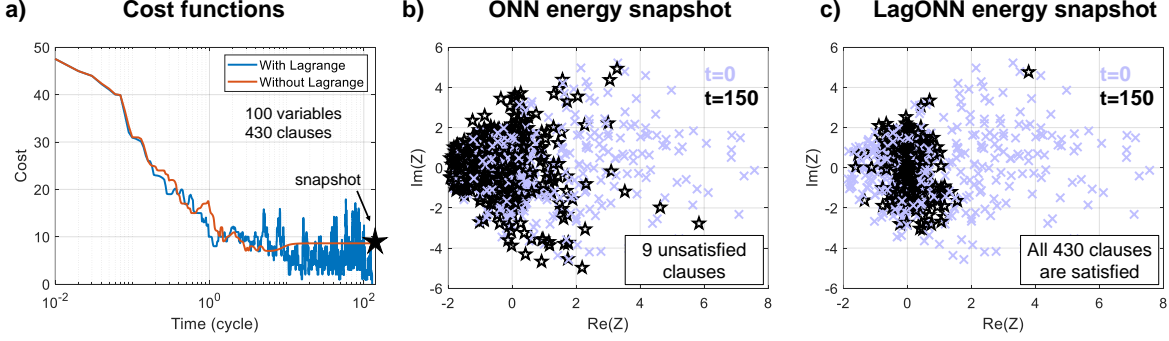


Figure 7: Simulation for the satisfiable SATlib instance ‘cnf-100-01’ with $N = 100$ variables and $M = 430$ clauses. Here, we monitor the cost function and stop the simulation when the cost < 0.125 or when the system reaches a fixed point. a) Cost function comparison between the standard ONN and the Lagrange version. While the two systems produce a rapid cost decrease in about 1 oscillation cycle (with more than 35 satisfied clauses), Lagrange oscillators are then actively exploring the phase space when the standard ONN gets stuck into a local minimum. When the Lagrange ONN finds an optimal phase assignment at $t=150$ oscillation cycles, we take a snapshot of all energy terms Z_m . b) Standard ONN energy snapshot. The black stars show the energy values at the snapshot time. Most of them are not settling to the target $Z_m = 0$. c) LagONN energy snapshot. When the simulation is stopped (cost < 0.125), Z_m values are getting closer to the origin. By monitoring the cost in real-time, we do not need to wait for full convergence towards an optimal saddle point where all $Z_m = 0$.

A LagONN cost function

From the SATlib .cnf files [38], we build a system of differential equations for each instance (Eq. 16). As there is no straightforward Lyapunov function for the system, we monitor the number of unsatisfied clauses in real-time using a custom cost function $\kappa(\phi)$ defined as:

$$f_B = C_1 \bigwedge C_2 \bigwedge \dots \bigwedge C_{M-1} \bigwedge C_M \\ \longrightarrow \kappa(\phi) = K_1 + K_2 + \dots + K_{M-1} + K_M$$

where $K_m(\phi) = l_1^m l_2^m l_3^m$ with literals $l_j^m = 0.5(1 \pm \tanh(\beta \cos \phi_j^m)) \in [0, 1]$. The sign that weights the tanh term depends on whether the literal l_j^m corresponds to a positive x_j (-) or negated variable \bar{x}_j (+). This way, $K_m(\phi) = 0$ if there is a variable assignment that satisfies the clause C_m . Consequently, f_B is true if $\kappa(\phi) = 0$. The tanh function is used to map phases to Ising spin values and is equivalent to rounding phases to the nearest multiples of π . For a sufficiently high β -value, we then have $\kappa(\phi) = N_{\text{unsat}}$, i.e. $\kappa(\phi)$ counts the number of unsatisfied clauses. Note that with the proposed rounding procedure, a clause C_m is true if and only if $K_m(\phi) < 0.5^3 = 0.125$ ($K_m(\phi) = 0.125$ when $\forall j \cos \phi_j^m = 0$). Thus, if $\kappa(\phi) < 0.125$, f_B is true and we use this value as a threshold to stop the LagONN search as shown in Fig. 7a. for $N = 100$ variables and $M = 430$ clauses. In this example, the nominal ONN case gets stuck in a state with 9 unsatisfied clauses around 10 oscillation cycles. In contrast at a similar time, LagONN’s cost trace fluctuates between low-cost values, highlighting that LagONN actively searches for an optimal assignment. Interestingly, LagONN’s search does not seem to have a detrimental impact on its initial cost reduction but continues exploring low-cost states. Fig. 7b and c show the energy values Z_m for each clause at the initialization (purple cross) and at the snapshot time $t=150$ oscillations (black star) when LagONN finds an optimal solution. For the nominal ONN, the final fixed point does not satisfy $Z_m = 0$ for many clauses. Since we do not wait for the full network convergence, many LagONN’s final Z_m values also differ from 0 but are closer to the origin acting as an attractor. Again, this example shows there is no need to wait for the full system convergence. Note that without Lagrange oscillators, it is guaranteed that the system will converge since it has a Lyapunov function [17]. However, for LagONN, there is no convergence guarantee due to the gradient ascent operated by the Lagrange oscillators. In practice, one could have a standard Boolean circuit corresponding to the formula f_B (with AND and OR gates) checking in real-time the number of satisfied clauses and sampling the phases when the cost reaches some target value.

B ODE solver for LagONN’s state equations

To study the stiffness of LagONN’s state equations, we first employed a custom ODE solver with an adaptive time-step to get time-step statistics in Matlab. We chose Fehlberg’s method, which has a local error scaling as $O(dt^4)$ and requires

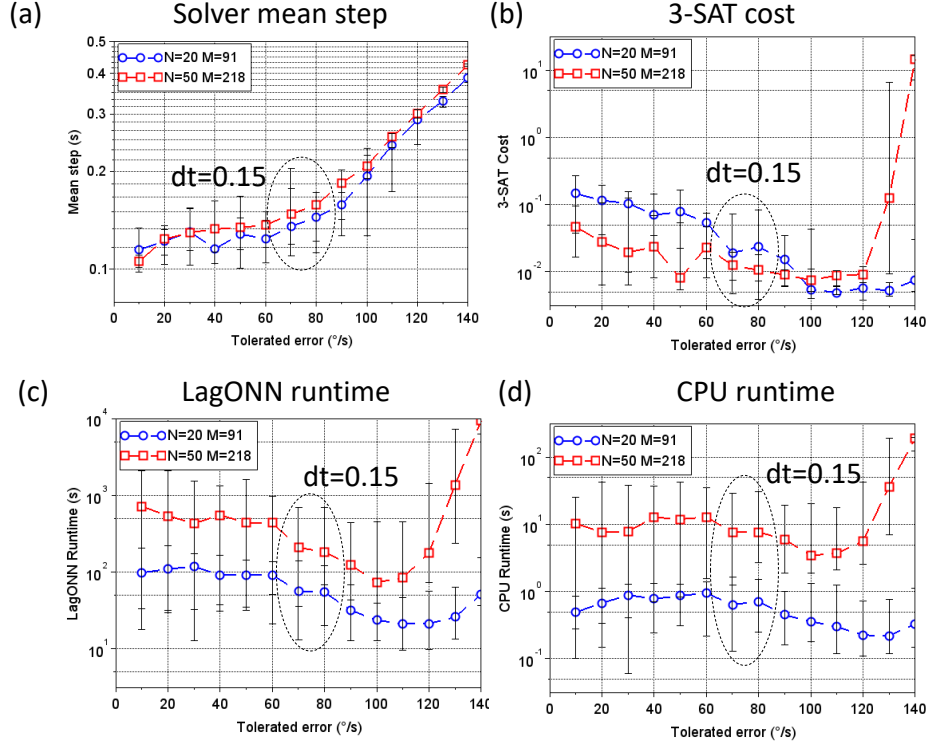


Figure 8: a) Median solver step versus the tolerated phase error ϵ for 10 3-SAT instances with $(N, M) \in (20, 91), (50, 218)$. Error bars correspond to 1st and 3rd quartiles. b) 3-SAT cost vs. tolerated error. c) LagONN runtime vs. tolerated error. d) CPU runtime vs. tolerated error.

three evaluations of $\nabla L_T(\phi)$ per time step and hence is a good compromise between speed and accuracy. It consists of a predictor/corrector method that provides a local error estimate at each time step which is then used to adapt the step size. The predictor phase values ϕ_p are first computed according to Heun's method as:

$$\phi_p[k+1] = \phi[k] + dt[k] \times (f_1 + f_2)/2 \quad (20)$$

where $f_1 = \nabla L_T(\phi[k])$ and $f_2 = \nabla L_T(\phi[k] + dt[k] \times f_1)$.

The corrector phase values are then calculated according to Simpson's rule as:

$$\phi[k+1] = \phi[k] + dt[k] \times (f_1 + f_2 + 4f_3)/6 \quad (21)$$

where $f_3 = \nabla L_T(\phi[k] + dt[k] \times (f_1 + f_2)/4)$. We estimate the local error as:

$$e_r = \sqrt{\frac{(\phi_p - \phi) \times (\phi_p - \phi)^T}{N + M}} \quad (22)$$

where N and M are the number of variables and clauses. Given a target error ϵ in rad/s, the new time step is calculated as:

$$dt[k+1] = 0.9 dt[k] \Gamma \quad (23)$$

with $\Gamma = \sqrt{dt[k]\epsilon/e_r}$. If $\Gamma < 1$, the solver reiterates with a smaller time step. Otherwise, it integrates the next point with a larger time step. We varied the tolerated error $\epsilon \leq 140^\circ$ using 10 instances per size $N = 20$ and $N = 50$ from the SATlib library [38]. Each LagONN instance was run 100 times with random initialization. Fig.8a shows the solver mean step size that exponentially increases with the tolerated error ϵ .

Surprisingly, LagONN is robust to numerical errors since it still finds optimal solutions with a similar runtime up to $\epsilon = 100^\circ$ (Fig.8b and c). LagONN's runtime even decreases with numerical error, down to $10\times$ for $N = 50$. However, when $\epsilon > 100^\circ$, i.e. $< dt > \approx 0.2$, LagONN's runtime explodes for $N = 50$. Based on this study, we ran our custom solver with a fixed time step $dt = 0.15$ for all simulations in the paper. The Matlab code was executed on a Linux server using one CPU per run.

C Simulated annealing algorithm

In this paper, we execute SASAT, the simulated annealing algorithm proposed in [66] for SAT and expressed as follows:

Algorithm 1: SASAT Algorithm [66]

Input: A set of clauses with N variables, MAX_TRIALS , MAX_TEMP , and MIN_TEMP

Output: A variable assignment S

```

1  $trial \leftarrow 1$ ;
2  $decay\_rate \leftarrow 0.2/N$ ;
3 while  $trial \leq \text{MAX\_TRIALS}$  do
4    $S \leftarrow$  a random variable assignment;
5    $j \leftarrow 0$ ;
6    $T \leftarrow \text{MAX\_TEMP}$ ;
7   while  $T \geq \text{MIN\_TEMP}$  do
8     if  $S$  satisfies the clauses then
9       return  $S$ ;
10     $T \leftarrow \text{MAX\_TEMP} \cdot \exp(-j \cdot decay\_rate)$ ;
11    for  $i \leftarrow 1$  to  $N$  do
12      Compute the cost change  $\delta$  in the number of unsatisfied clauses if  $i$  is flipped;
13      Flip  $i$  with probability  $1/(1 + \exp(\frac{\delta}{T}))$ ;
14       $S \leftarrow$  the new assignment if flipped;
15     $j \leftarrow j + 1$ ;
16   $trial \leftarrow trial + 1$ ;

```

The temperature decay rate was adjusted heuristically and scaled with the number of variables as $decay_rate = 0.2/N$ to increase the annealing time and the success probability for larger instances. We have set $\text{MAX_TEMP}=1$ and $\text{MIN_TEMP}=0.01$ for all the experiments by inspecting the cost trace for several sizes.

D LagONN saddle points and dynamics

D.1 Optimal saddle point

Here we prove Theorem 2 which generalizes Theorem 1 to M clauses.

Theorem 2. Let $L_T(\phi, \phi_\lambda) = \sum_m^M u_\lambda^m \cdot \vec{Z}_m$ and the formula $f_B = C_1 \wedge C_2 \wedge \dots \wedge C_{M-1} \wedge C_M$ is satisfiable, then:

1. L_T has at least one saddle point $L_T(\phi^*, \phi_\lambda^*) = 0$ such that $L_T(\phi^*, \phi_\lambda) \leq L_T(\phi^*, \phi_\lambda^*) \leq L_T(\phi, \phi_\lambda^*)$.
2. Such saddle point satisfies the constraints $Z_m(\phi^*) = 0$ for all clauses.

Proof. 1. We motivate the search for a saddle point using the concept of *duality* [63]. Consider the following dual function defined as:

$$D_T(\phi_\lambda) = \min_{\phi} L_T(\phi, \phi_\lambda) \quad (24)$$

For any vector of phases ϕ_λ it is possible to find an optimal assignment of phase ϕ^* such that constraints are satisfied, i.e. for all clauses $Z_m = 0$ which gives as optimal value $L_T(\phi^*, \phi_\lambda) = 0$. Hence, $D_T(\phi_\lambda) \leq 0$. The dual problem consists of finding the best lower bound for the optimal value of the initial problem — that is satisfying the constraints $Z_m = 0$ for all clauses C_m . Hence, we are looking for ϕ_λ that maximizes $D_T(\phi_\lambda)$ as:

$$\max_{\phi_\lambda} D_T(\phi_\lambda) = \max_{\phi_\lambda} \min_{\phi} L_T(\phi, \phi_\lambda) \quad (25)$$

For any ϕ , we can find a vector of phases ϕ_λ such that their corresponding unitary vectors are orthogonal to their corresponding \vec{Z}_m , hence, $\max_{\phi_\lambda} \min_{\phi} L_T(\phi, \phi_\lambda) = 0$. Consider now the inverse situation where we first maximize L_T as:

$$P_T(\phi) = \max_{\phi_\lambda} L_T(\phi, \phi_\lambda) \quad (26)$$

For any ϕ , we can set the phases ϕ_λ such that their corresponding unitary vectors point in the same direction as their \vec{Z}_m . Hence, $P_T(\phi) \geq 0$. Seeking the best higher bound is expressed as:

$$\min_{\phi} P_T(\phi) = \min_{\phi} \max_{\phi_\lambda} L_T(\phi, \phi_\lambda) \quad (27)$$

For any ϕ_λ , the best higher bound $P_T(\phi)$ is obtained when all the constraints are satisfied, i.e. $Z_m = 0$ for all clauses C_m . Hence, $\min_{\phi} \max_{\phi_\lambda} L_T(\phi, \phi_\lambda) = 0$. In summary, we obtain:

$$L(\phi^*, \phi_\lambda^*) = \max_{\phi_\lambda} \min_{\phi} L_T(\phi, \phi_\lambda) = \min_{\phi} \max_{\phi_\lambda} L_T(\phi, \phi_\lambda) = 0 \quad (28)$$

Since L_T is continuous in both ϕ and ϕ_λ , and $L(\phi^*, \phi_\lambda^*)$ is attained for the satisfiable assignment of phase $\phi^* \in \{0; \pi\}^N$, $L(\phi^*, \phi_\lambda^*)$ is a saddle point satisfying the inequality $L_T(\phi^*, \phi_\lambda) \leq L_T(\phi^*, \phi_\lambda^*) \leq L_T(\phi, \phi_\lambda^*)$.

2. By contradiction, suppose that (ϕ^*, ϕ_λ^*) is a saddle point of L_T satisfying $L_T(\phi^*, \phi_\lambda) \leq L_T(\phi^*, \phi_\lambda^*) \leq L_T(\phi, \phi_\lambda^*)$, but there is some clause m such that $Z_m \neq 0$. Let us consider the corresponding Lagrange oscillator u_λ^m : the term $u_\lambda^m \cdot \vec{Z}_m$ is maximum when u_λ^m points in the same direction as \vec{Z}_m . If at the saddle point u_λ^m is not already pointing in the same direction as \vec{Z}_m , we can find a new Lagrange phase $\hat{\phi}_\lambda$ for this clause such that $L_T(\phi^*, \hat{\phi}_\lambda) > L_T(\phi^*, \phi_\lambda^*)$, which violates the saddle condition $L_T(\phi^*, \phi_\lambda) \leq L_T(\phi^*, \phi_\lambda^*)$ for all ϕ_λ . If at the saddle point, the vector u_λ^m with phase ϕ_λ^* points in the same direction as its respective $\vec{Z}_m \neq 0$, we can find a new assignment of phase $\hat{\phi}$ satisfying all constraints and $Z_m = 0$ such that $L_T(\phi^*, \phi_\lambda^*) > L_T(\hat{\phi}, \phi_\lambda^*)$, violating the saddle condition $L_T(\phi^*, \phi_\lambda^*) \leq L_T(\phi, \phi_\lambda^*)$ for any ϕ .

□

D.2 Proposed dynamics to find a saddle point

To find an optimal saddle point as described by Theorem 2, we combine gradient descent and ascent along ϕ and ϕ_λ :

$$\begin{cases} \tau \dot{\phi}_x = -\nabla_{\phi_x} L_T \\ \tau_\lambda \dot{\phi}_\lambda = +\nabla_{\phi_\lambda} L_T \end{cases} \quad (29)$$

Under these dynamics, the Lagrange function is not a Lyapunov function for the system since with our proposed dynamics L_T can increase with time (gradient ascent along ϕ_λ). Focusing on a single clause i , its time derivative is indeed expressed as:

$$\frac{dL_i}{dt} = \frac{d\vec{u}_\lambda}{dt} \cdot \vec{Z}_i + \frac{d\vec{Z}_i}{dt} \cdot \vec{u}_\lambda \quad (30)$$

and L_i 's gradient descent causes \vec{Z}_i to evolve in the opposite direction from \vec{u}_λ as expressed here for $\tau = 1$:

$$\begin{aligned} \frac{d\vec{Z}_i}{dt} \cdot \vec{u}_\lambda &= \frac{\partial \vec{Z}_i}{\partial \phi_X} \cdot \vec{u}_\lambda \frac{d\phi_X}{dt} + \frac{\partial \vec{Z}_i}{\partial \phi_Y} \cdot \vec{u}_\lambda \frac{d\phi_Y}{dt} + \frac{\partial \vec{Z}_i}{\partial \phi_Z} \cdot \vec{u}_\lambda \frac{d\phi_Z}{dt} \\ &= -\left(\frac{\partial \vec{Z}_i}{\partial \phi_X} \cdot \vec{u}_\lambda\right)^2 - \left(\frac{\partial \vec{Z}_i}{\partial \phi_Y} \cdot \vec{u}_\lambda\right)^2 - \left(\frac{\partial \vec{Z}_i}{\partial \phi_Z} \cdot \vec{u}_\lambda\right)^2 \\ &\leq 0 \end{aligned} \quad (31)$$

whereas L_i 's gradient ascent tends to bring \vec{u}_λ towards \vec{Z}_i as:

$$\begin{aligned} \frac{d\vec{u}_\lambda}{dt} \cdot \vec{Z}_i &= \frac{\partial \vec{u}_\lambda}{\partial \phi_\lambda} \frac{d\phi_\lambda}{dt} \cdot \vec{Z}_i \\ &= (\vec{Z}_i \cdot \vec{u}_\lambda)^2 \\ &\geq 0 \end{aligned} \quad (32)$$

E Impact of Lagrange oscillator speed

Throughout the paper, we assumed that the Lagrange and the standard oscillators are equally fast, i.e. $\tau = \tau_\lambda = 1$ in Eq. 16. Here, we study how speeding up or slowing down the Lagrange oscillators affects the runtime of the whole network. In particular, we set $\tau = 1$ and vary τ_λ for the Lagrange oscillator and measure the resulting time-to-solution (TTS) (see Eq. 17).

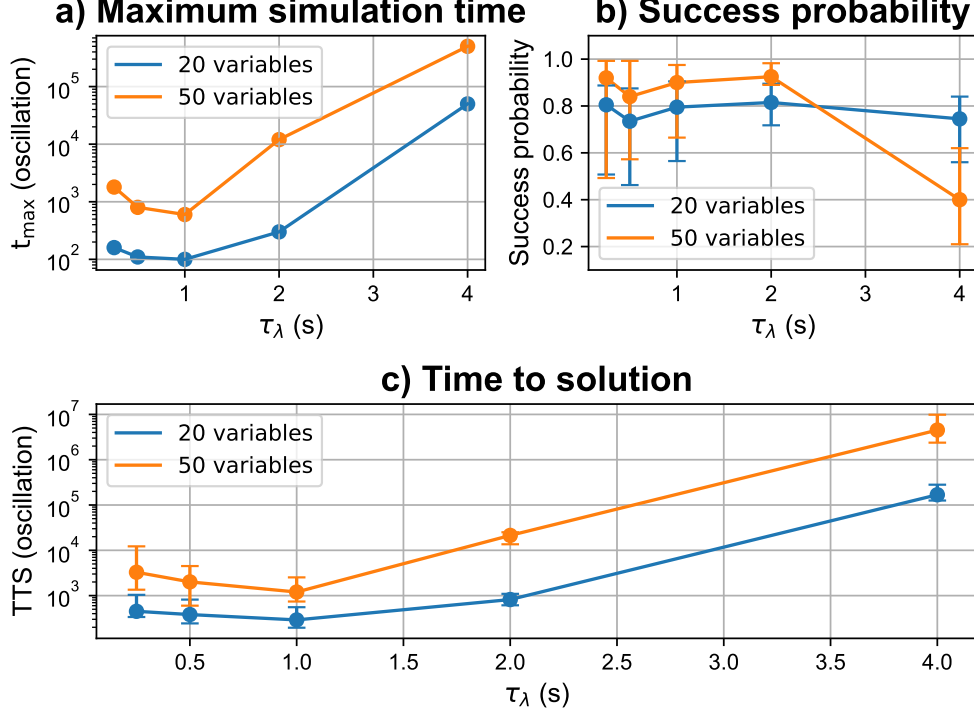


Figure 9: Impact of different τ_λ on the time-to-solution of LagONN. Here a simple benchmark on the Max-3-SAT problem with 20 and 50 variables for 20 instances each and 100 trials per instance. a.) Maximum simulation time as a function of τ_λ for 20 and 50 variables. b.) Median success probability p_s as a function of τ_λ for 20 and 50 variables. c.) Median time to solution as a function of τ_λ for 20 and 50 variables.

Here we use the first 20 instances from SATlib with 20 and 50 variables with 100 trials for each instance. For each τ_λ , we set a maximum simulation time t_{max} . Next, we check whether each trial finds an optimal solution in the predetermined simulation time. Based on these results, we compute the median success probability p_s for each τ_λ . Combining the maximum simulation time and the success probability, we can quantify the median time to solution for 20 and 50 variables for each τ_λ value. The results are summarized in Fig. 9.

For minimum TTS, there seems to be an optimal value for $\tau_\lambda \approx 1$, which means all oscillators should have the same speed. Although more rigorous analysis is needed, $\tau_\lambda/\tau = 1$ may be linked to the saddle geometry of the optimal point (Theorem 2), where minimization and maximization are interchangeable and maximization does not need to be performed in an outer loop as a slower process.

F Discretization of LagONN dynamics

To lay the groundwork for a potential LagONN digital hardware implementation, here we study the effect of phase discretization on the dynamics. We discretize the phase interval from 0 to 2π with a fixed number of states N_{states} . For example for $N_{states} = 16$ the phases can take on values

$$\phi = \frac{2\pi}{16}k, \quad (33)$$

with k an integer from 0 to $N_{states} - 1 = 15$. We study $N_{states} = 16, 32, 64, 128, 256, 512, 1024, 2048, 4096, 8192$ and run LagONN simulations on the first 20 instances from SATlib for 20 variables and 91 clauses, and for 50 variables and 218 clauses. Each instance is given 100 trials with random initial phases. We used the same random initial phases per trial, except discretized to the corresponding N_{states} . The time-to-solution metric, as defined in Eq. 17, is used to compare different discretization levels. The results are shown in Fig. 10. For the case of 50 variables with $N_{states} = 16$ or $N_{states} = 32$, the data points are excluded due to unstable behavior.

As can be seen in Fig. 10, there is a strong increase in time to solution below $N_{states} = 64$ for instances with 20 variables, after which the TTS flattens. For 50 variables, the same can be seen, except that the trend flattens after around

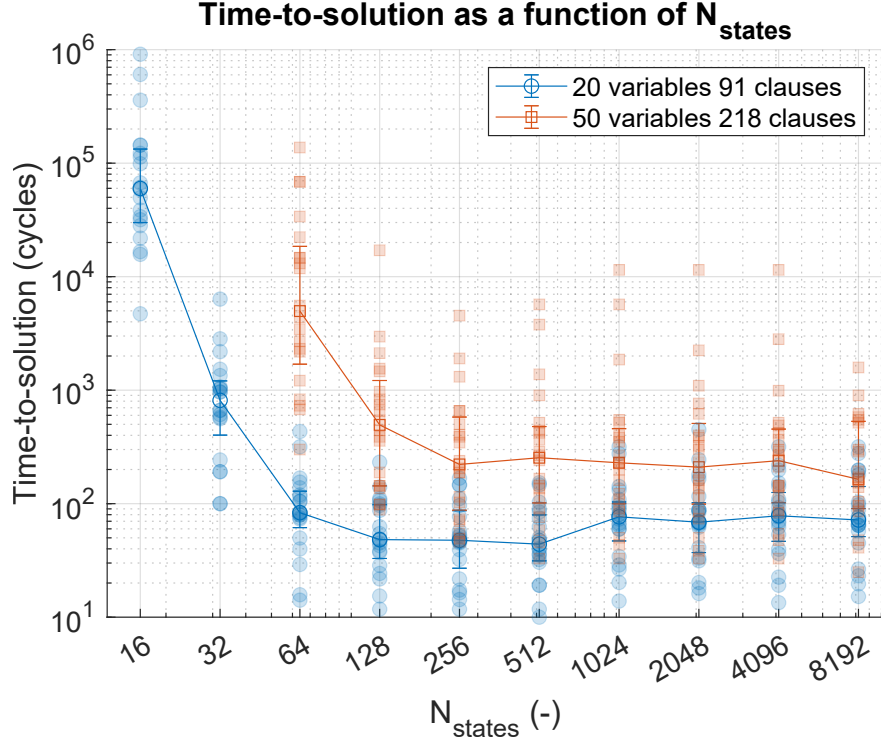


Figure 10: Performance scaling when discretizing the phase dynamics of LagONN to different number of states N_{states} . The median runtimes are shown with the 25% and 75% quantiles as error bars.

$N_{\text{states}} = 128$. We can conclude from these results that for a digital implementation of LagONN, one should take care to discretize the phases to a sufficiently high number of states to obtain a stable system. For 20 variables, this will be around $N_{\text{states}} \geq 64$, while for 50 variables it is around $N_{\text{states}} \geq 128$. Although more data is needed, we hypothesize that a higher number of variables beyond 50 would also require a higher number of N_{states} .